

## **Response to reviewer #1**

### *General comments*

*The study by Ueda et al. addresses the effect of coatings on the absorptive properties of atmospheric black carbon particles, which is important in evaluating their radiative impacts. The authors conducted a field campaign at Noto Peninsula, Japan, a site that frequently receives pollutants transported from mainland China. A variety of instruments, including PASS-3, SP2, SMPS, and TEM were employed to measure the physical, chemical, optical, and morphology of aerosols. NO<sub>x</sub> and NO<sub>y</sub> were also measured to assist photochemical age determination. The main conclusion is that coatings on black carbon particles can enhance the absorption by uncoated black carbon by ~22%. This observation adds to the limited database on field measurements of the lensing effect of black carbon. The measurement and discussion are generally sound but a number of details need to be added or explained, most importantly the charring of aerosols in the thermodenuder and its impact on the absorption enhancement measurements. I recommend publication of this manuscript after the following concerns are addressed.*

(reply)

We appreciate the valuable comments from the reviewer. We have considered the comments carefully and replies are described below.

### *Specific comments*

*1. Abstract, L13, the absorption enhancement is 22-23%. This is not a range. I suggest to report either 22% or 23%. The same comment applies to the Eabs of 1.22 – 1.23 in the conclusion. In addition, please either use percentage or absolute numbers to be consistent throughout the text.*

(reply)

We have corrected the descriptions on the average absorption enhancement value throughout the text in the revised manuscript.

*2. Please use “thermodenuder” instead of “heater” throughout the text to be consistent with literature in this field.*

(reply)

We have replaced the “heater” with “thermodenuder”.

*3. Abstract, L21-22, it is a bit surprising that most of the coatings on black carbon are sulfates,*

*given that organic materials dominate the aerosol mass (Table 2). The measurement period is after the intense coal burning season in northern China, so it is expected that the coatings are dominated by organics.*

(reply)

Yes, coating materials should include not only sulfate but also organics. In the EDS analysis, the quantitative detection of C atoms is difficult due to the large background signal from C-coated collodion film. Therefore, there is a possibility that the number of C-rich particles is actually higher than that counted, as described in section 2.3. We have revised the sentence as follows.

(original)

“The majority of the soot in all samples was found as mixed particles with spherical sulfate or as clusters of sulfate spherules. For samples showing high enhancement (>1.30) of BC light absorption, TEM showed that the internally mixed soot-containing particles tended to have a more spherical shape and to be thickly-coated.”

(revised)

“The majority of the soot in all samples was found as mixed particles with sulfate-containing spherules or as clusters of such spherules. For samples showing high enhancement (>1.30) of BC light absorption, TEM showed that the internally mixed soot-containing particles tended to have a more spherical shape and to be embedded into the sulfate.”

4. P25093, “*Models often estimate  $E_{\text{abs}}$  assuming a core-shell...*” *Many models simply apply a constant  $E_{\text{abs}}$  value rather than estimating  $E_{\text{abs}}$ .*

(reply)

We have revised the sentence according to the comment.

(original)

“Models often estimate  $E_{\text{abs}}$  assuming a core-shell (the BC core and coating materials) shaped spherical particle (Bond et al., 2006; Ma et al., 2012)”

(revised)

“Models often apply a constant  $E_{\text{abs}}$  value or estimate  $E_{\text{abs}}$  assuming a core-shell (the BC core and coating materials) shaped spherical particle (Bond et al., 2013 and references therein)”

5. P25093, *the last paragraph. What are the values reported from these previous  $E_{\text{abs}}$  measurements? These values should be summarize here. In addition, two recent studies that address  $E_{\text{abs}}$  via field measurements are missing and should be added to the summary: “Healy, R. M., et al.*

(2015), *Light-absorbing properties of ambient black carbon and brown carbon from fossil fuel and biomass burning sources*, *J. Geophys. Res. Atmos.*, 120, 6619–6633, doi:10.1002/2015JD023382” and “Liu, S. et al. *Enhanced light absorption by mixed source black and brown carbon particles in UK winter*. *Nat. Commun.* 6:8435 doi: 10.1038/ncomms9435 (2015).”

(reply)

We have added the values of the enhancement of light absorption due to coating and these new literatures in the revised manuscript.

6. P25093-25094, “However, these studies were conducted ... has been reported.” The Liu et al. study mentioned above was conducted at a rural site and measured aged air masses. That study also combines optical and morphology measurements. Therefore the author’s statements need to be removed or changed.

(reply)

We have revised these sentences in the revised manuscript as follows.

(original)

“However, these studies were conducted in or around urban areas; therefore, the contribution of the lensing effect in a well-aged air mass remains unclear. In addition, to our knowledge, no direct comparison of the observed lensing effect with the particle morphology of individual BC-containing particles has been reported.”

(revised)

“However, there have been very few observational studies reported the contributions of lensing effect and their relation with morphology of individual BC-containing particles in a well-aged air mass.”

We have also added the following sentences in the discussion section of the revised manuscript.

“Very recently, Liu et al. (2015) reported the average  $E_{\text{abs}}(781 \text{ nm})$  of 1.4 for BC particles emitted from fossil fuel and residential burning sources in winter at a rural site, Detling (45 km away from London) in UK. The average  $E_{\text{abs}}(781 \text{ nm})$  value obtained in the present study is slightly lower than the value reported by Liu et al. (2015).”

7. P25094, the second paragraph is not discussing absorption enhancement and is not closely related to the paragraphs before and after, this paragraph should be moved forward where the concept of black carbon is introduced.

(reply)

According to the comment, this paragraph has been moved forward in the revised manuscript.

8. *P25095, the CE of 0.3 is very low compared to the typical CE of 0.5. It says the CE was derived by comparing the mass concentration of the ACSM data with filter data, but how the filter sample was collected is not clear, e.g., what is the duration of the sample collection, what is the size cut of the filter measurements, was the filter weighed to get the mass concentration. In addition, the ACSM does not measure refractory components, while the weight of the filter is a sum of all materials on the filter. This could result in a low CE.*

(reply)

The filter samples were collected using a 9-stage Andersen sampler (model AN-200, Tokyo Dylec corp.) with a flow rate of 28.3 L/min. Sampling duration was 1 week per sample. The mass concentration was not obtained by weighing the filter. Instead, the filters were extracted and water soluble inorganic components were analyzed by ion chromatography. Ammonium and sulfate concentrations were integrated for the smallest 3 stages (including backup filter) to obtain the PM1.1 fraction. The CE was tuned so that the ACSM derived ammonium and sulfate match the filter based analysis. We have added the information in the revised manuscript.

9. Related to the question above, the CE can also be derived by comparing ACSM with SMPS measurements. Since the SMPS data are available, this approach should be tested and may result in a different CE.

(reply)

According the comment, the volume concentrations of NR components have been calculated using the ACSM data and were compared to volume concentrations estimated using the SMPS data. The volume concentrations estimated from SMPS data are found to be about 1.7 times larger than those calculated from ACSM data. While different size-cut profiles of the ACSM, Andersen sampler, and SMPS may have affect the result, measurement uncertainty of SMPS may also contribute to the difference. It should be noted that selection of the CE value itself does not affect the discussion in this study. We have added the information in the revised manuscript.

10. *P25096, more details about the thermodenuder should be added, e.g., what are the dimensions of the denuder? What is the residence time of particles in the denuder? These are important features as a short residence time will result in incomplete removal of the coating materials on BC.*

(reply)

The same type of TDs used in a previous study (Guo et al., 2014; Nakayama et al., 2014) was used in this study. The TD consists of a stainless tube (outer and inner diameters: 12.7 and 10.2 mm, respectively; length: 600 mm) and electronic jacket heaters (Heater Engineer, P-series). Flow rates through the TD was 1.28 lpm, and the residence time for the sample aerosols in the TD was estimated to be 2.3 s, on the assumption of plug flow conditions (at 20°C). We have added the information in the revised manuscript.

11. P25097, *it is surprising that there is no particle loss in the thermodenuder as the ratio is not significantly different than 1. This is inconsistent with many previous studies, e.g., the Cappa et al. 2012 paper cited in the manuscript and the references therein. Could this be due to the generation of brown carbon in the thermodenuder? This could be a critical problem as it affects the calculation of  $E_{\text{abs}}$ .*

(reply)

The ratios of mass concentration of rBC measured by the SP2 without heating to that after heating (1.08 and 1.03 at 300 °C and 400 °C, respectively, on average) include contributions of both loss and formation of rBC in the TD. Considering the estimated particle loss in our TD, ~17% and ~20% at 300 °C and 400 °C, respectively (Guo et al. 2014), our results suggest that non-negligible amount of rBC (10-20% of ambient rBC) were formed in the TD, possibly due to charring by heating. In the present study, the  $E_{\text{abs}}$  values were estimated by taken these effects into account, assuming that light absorbing property of ambient rBC is same with that of rBC generated in the TD and detected by the SP2, using the equation,

$$E_{\text{abs}}(\lambda, T) = \frac{b_{\text{abs}}(\lambda, 25^\circ\text{C})/b_{\text{abs}}(\lambda, T)}{m_{\text{rBC}}(25^\circ\text{C})/m_{\text{rBC}}(T)},$$

where  $\lambda$  and  $T$  were measurement wavelength and TD temperature, respectively. If mass absorption cross section at 781 nm for rBC generated in the TD would be different by 50% with that for ambient rBC, the lensing effect could be underestimated or overestimated by 0.05-0.10. The information and equation to calculate  $E_{\text{abs}}$  have been added in the revised manuscript (sections 2.2 and 3.1).

12. P25097, L1, *references are needed after “scattering signal”.*

(reply)

A reference (Moteki and Kondo. 2007) has been added in the revised manuscript.

13. P25097, was a NO<sub>2</sub> scrubber installed upstream of the PASS-3 instrument? If not, NO<sub>2</sub> could influence the absorption measurement at 405 nm and also the E<sub>abs</sub> calculation at 405 nm. This needs to be examined as it may influence the hypothesis of brown carbon formation in the thermodenuder.

(reply)

The influence of light absorption of NO<sub>2</sub> has been evaluated based on the estimation using transmittance of NO<sub>2</sub> through filter and inlet tube as well as mixing ratio of NO<sub>2</sub>, and confirmed to be small (<0.05 Mm<sup>-1</sup> at 405 nm and <0.04 Mm<sup>-1</sup> at 532 nm). The effects have been taken into account for the determination of  $b_{\text{abs}}$  in the revised manuscript. The information has been added.

14. P25097, the detection limit of the PASS-3 measurements. Are the data reported as 3-h averages, e.g., the data presented in Fig. 2? If not, the detection limit should be calculated using data with the same time resolution as the real measurements.

(reply)

Yes, we used 3-h averages data in Fig. 2 and Fig. 3. This explanation has been added in caption of Fig. 2.

15. P25097, “Using  $b_{\text{abs}}$  values after the above ratios,” it is not clear what this sentence means. In addition, how was the particle loss accounted for?

(reply)

As described in the reply for the comment 11, contributions of both loss and formation of rBC in TD were taken into account. We have corrected the sentence and added the equation to estimate  $E_{\text{abs}}$  in the revised manuscript.

16. P25099, L11, “a prior test”. What test is it? When was the test? More information is needed here.

(reply)

The description was not correct. We used spectra for non-particle areas measured between each sample analysis as background spectra. This sentence has been revised as follows.

(original)

“In this classification, a spectrum larger than two times the standard deviation of the background spectra measured in a prior test was used as the detectable spectrum of the particles to eliminate

background noise effects”

(revised)

“In this classification, a spectrum larger than two times the standard deviation of the background spectra, which are spectra for non-particle areas measured between each sample analysis, was used as the detectable spectrum of the particles to eliminate background noise effects.”

17. P25100, “the  $E_{abs}$  values at all wavelengths are expected to be greater than 1.0”. This is not true given the sequential bypass and thermodenuder measurements in this study. Values smaller than 1.0 are likely due to the atmospheric variability the BC concentration.

(reply)

As commented by the reviewer, we cannot rule out the possible contributions of the temporal variation of BC concentration to the variation in  $E_{abs}$  values, while the observed wavelength dependence of  $E_{abs}$  values cannot be explained by the temporal variation of BC concentration. We have removed this sentence in the revised manuscript.

18. P25100, L17, “This can be explained by the increase of absorbing materials by heating.” The formation of brown carbon in thermodenuder is interesting, is there any literature on this topic? Later it says in P25112 that the formation of brown carbon is “probably due to the condensation of non-volatile organic.” Under the 300 – 400 C condition in the thermodenuder, how can condensation occur?

(reply)

Thank you for the valuable comment. While several literatures reported the charring of organic carbon by heating as described in section 2.2, to our knowledge, there is no report on the formation of brownish materials by heating. Although the formation process of brownish materials by heating is unclear, the brownish materials may not be generated by condensation but by incomplete charring process. We have revised the sentence in P25112 as follows.

(original)

“Therefore, the spherical, carbon-rich particles might be formed by heating, probably due to the condensation of non-volatile organic compounds within the particles, and could be brown in colour.”

(revised)

“Therefore, the spherical, carbon-rich particles might be formed by heating, probably due to the incomplete charring of organic compounds, and could be brown in colour.”

19. *Charring in the thermodenuder could produce elemental carbon, how can formation of elemental carbon be excluded? This could affect the calculation of  $E_{abs}$  at 781 nm, and could also be related to the observation that the  $E_{abs}$  at 781 nm is independent on  $NO_x$  to  $NO_y$  ratio.*

(reply)

As described in the reply for the comment 11, contributions of both loss and formation of rBC in TD were taken into account for the estimation of  $E_{abs}$ . Discussion on the possible contributions of for the formation of rBC by heating has been added in section 3.1 in the revised manuscript.

20. *P25101, L11, “north and west of the site.” There is a significant fraction of air mass coming from northeast section of the site.*

(reply)

We have removed the sentences in the revised manuscript.

21. *P25101, L25, the location of Shanghai should be added to the figure as it is the origin of air masses.*

(reply)

The location of Shanghai was already shown in Fig. 3a.

22. *P25103, L1-2, the photochemical age can be directly calculated using  $NO_x$  and  $NO_y$ .*

(reply)

Quantitative estimation of the photochemical age has been removed according to the Referee #2's comments.

23. *P25104, L14, “a mechanical issue”, it is not clear what issue results in the inability to calculate BC coating thickness.*

(reply)

Mechanical issue is that one of detectors in the SP2 did not work well. This detector can measure the scattering light signal to estimate the absolute position of particles in the laser beam, we called “split detector”, which is important information to conduct the fitting to estimate the BC coating thickness. Therefore, we could not obtain the BC coating thickness, unfortunately. We have added the information.

24. P25105-25111, section 3.3.2 and 3.3.3. There is a vast amount of information in these two sections (6.5 pages). While the information is useful to understand the aerosol properties, much is not related to the absorptive properties of BC, which is the theme of this paper. I think these two sections can be substantially shortened, or some information and related figures can be moved to SI information so that the main text is more succinct.

(reply)

According to the reviewer's comments, some information, one table, and one figure in section 3.3.2 and 3.3.3 were moved to supplemental materials (S2-S4).

25. Fig 1 e-f, the green and blue traces cannot be differentiated visually. Please make separate panels.

(reply)

We have remade the figure, according to the comment.

#### *Technical corrections*

1. Abstract, L14, change "under high absorption coefficient conditions" to "under high absorption coefficient periods"
2. Abstract, L18, remove "coefficient"
3. P25092, L12, change "defined operationally" to "operationally defined"
4. P25093, change "noncoated" to "uncoated"
5. P25093, L22, change "estimated" to "measured"
6. P25094, L18, change "absorbing" to "absorption"
7. P25094, L19, remove "suspended in air"
8. P25098, L5, remove "a"

(reply)

According to the reviewer's comments, we revised above all technical corrections.

## **Response to reviewer #2**

*The authors study black carbon (also called soot) collected in Noto Peninsula, Japan. SP2 was used to evaluate the particle absorption of soot-containing particles under ambient air and through one heater denuder. The study found absorption enhancement have not changed or decrease after the heating process. The phenomenon is contrast to the expectation. The TEM was employed to observe the particles and provided the direct the evidence here. They found that the heating process can make particle charring and brownist which can enhance particle absorption in short wavelength. Finally, the authors suggest the 781 nm was selected to reflect soot coating/shell.*

*In this study, the authors also characterize the particle CF, AR, and RP. These parameters can indicate soot mixing structure. Also, these results can be used to explain the SP2 results. These results are interesting and improve the understanding the links between soot-containing particle optical properties and mixing state. I would like to make one minor revision before the paper can be published in ACP.*

(reply)

We appreciate the valuable comments from the reviewer. We have considered the comments carefully and replies are described below.

*P25092 L1 leeward – downwind*

(reply)

We have replaced the word according to the comment.

*P25097 Eabs should be expressed by on formular*

(reply)

We have added the equation to calculate the  $E_{abs}$  values.

*P25096 L10 what kind of diffusion dryers? After the dryer, what is the air humidity? Please give more description.*

(reply)

We have used diffusion dryers with silica gel and the relative humidity in the cell of the PASS-3 was lower than 11% throughout the observation period. We have added the information in the revised manuscript.

*P25098 In figure 1, what place can be installed the single particle sampler? Please mark it.*

(reply)

The sampling line for TEM analysis was placed downstream of the PM10 inlet. We have added the explanation in section 2.3. The lines for continuous measurement in Fig. 1 and the sampling line for TEM analysis were separated in downstream of the PM10 inlet to stabilize the flow rate of continuous measurement.

*P25098 L19-22 where did the authors used the experiments?*

(reply)

The sentence was not correct. We thank your comment. In this study, shapes of Pt/Pd shadow were used to discriminate morphological types, but we did not measure the shadow length and particle height. We have corrected the sentence.

*P25100 make definition for brownish particles*

(reply)

We have replaced the brownish particle with the brownish materials and added the definition at the first appearance, as follows.

“This can be explained by the increase of “brownish materials” by heating. Here, the “brownish materials” are defined as the materials which were generated by heating in the TD and had significant light absorption at shorter visible wavelengths, to distinguish with ambient brown carbon particles.”

*Section 3.2 it is difficult to understand the section. I would like to suggest the authors shorten this part. I know that the authors want to make source identification. But I don't think NO<sub>x</sub>/NO<sub>y</sub> can indicate the air aging because of the complicate the weather during the long-range transport. From the continent to japan over East China sea, the humidity, temperature changed a lot. Therefore, it is better to delete L11-22 P25101. Figure 3b should be removed. Other can be kept depending on the authors.*

(reply)

We have removed these sentences in section 3.2 in the revised manuscript, according to the comments. The quantitative estimation of the plume age using NO<sub>x</sub>/NO<sub>y</sub> data in section 3.3.1 has

also been removed in the revised manuscript.

*P25102 “In the present study, no clear negative correlation between the Eabs and the ratio of NOx to NOy was observed, although the Eabs was expected to increase in the aged air mass if BC was thickly coated during transport.” That’s why the authors could find good negative correction.*

(reply)

We have removed the sentence in the revised manuscript.

*3.3.2 section. Could the authors make more clear structure? For example, type 1 could be one paragraph. And next type 2...*

(reply)

We have moved most of the section to SI section according to the comments by Referee #1 and revised the structure of the manuscript.

*P25109 L 21 ile?*

(reply)

This should be “percentile”. We have corrected the word.

*Figure 2, make large clear and large graph.*

(reply)

This figure has been revised, according to the comment.

1 **Light absorption and morphological properties of soot-**  
2 **containing aerosols observed at an East Asian outflow site,**  
3 **Noto Peninsula, Japan**

4 **S. Ueda<sup>1,2</sup>, T. Nakayama<sup>1,3</sup>, F. Taketani<sup>4</sup>, K. Adachi<sup>5</sup>, A. Matsuki<sup>6</sup>, Y. Iwamoto<sup>6,7</sup>, Y.**  
5 **Sadanaga<sup>8</sup> and Y. Matsumi<sup>1,3</sup>**

6 [1]{Solar-Terrestrial Environment Laboratory, Nagoya University, Nagoya, Japan}

7 [2] {Now at Graduate School of Environmental Studies, Nagoya University, Nagoya, Japan}

8 [3] {Now at Institute for Space-Earth Environmental Research, Nagoya University, Nagoya,  
9 Japan}

10 [4]{Japan Agency for Marine-Earth Science and Technology, Yokohama, Japan}

11 [5]{Atmospheric Environment and Applied Meteorology Research Department,  
12 Meteorological Research Institute, Tsukuba, Japan}

13 [6]{Institute of Nature and Environmental Technology, Kanazawa University, Kanazawa,  
14 Japan}

15 [7]{Now at Faculty of Science Division I, Tokyo University of Science, Tokyo, Japan}

16 [8]{Graduate School of Engineering, Osaka Prefecture University, Osaka, Japan}

17  
18 Correspondence to: S. Ueda ([ueda-s@stelab.nagoya-u.ac.jp](mailto:ueda-s@stelab.nagoya-u.ac.jp)) and T. Nakayama  
19 ([nakayama@stelab.nagoya-u.ac.jp](mailto:nakayama@stelab.nagoya-u.ac.jp))

20  
21 **Abstract**

22 The coating of black carbon (BC) with inorganic salts and organic compounds can enhance  
23 the magnitude of light absorption by BC. To elucidate the enhancement of light absorption  
24 of aged BC particles and its relation to the mixing state and morphology of individual  
25 particles, we conducted observations of particles at an Asian outflow site in Noto Peninsula,  
26 Japan, in the spring of 2013. Absorption and scattering coefficients at 405, 532, and 781  
27 nm and mass concentrations/mixing states of refractory-BC in PM<sub>2.5</sub> were measured using  
28 a three-wavelength photoacoustic soot spectrometer and a single-particle soot photometer

(SP2), respectively, after passage through a **thermodenuder (TD)** maintained at 300 °C or 400 °C or a bypass line maintained at room temperature (25 °C). The average enhancement **factor** of BC light absorption due to coating was estimated by comparing absorption coefficients at 781 nm for particles that with and without passing through the **TD at 300 °C** and was found to be **1.22**. The largest enhancements (**>1.30**) were observed under high absorption coefficient **periods** when the air mass was long-range transported from urban areas in China. Aerosol samples were also analyzed using a transmission electron microscope (TEM) equipped with an energy dispersive X-ray analyzer. The morphological features and mixing states of soot-containing particles of four samples collected during the high absorption events were analyzed by comparing microphotographs before and after the evaporation of beam-sensitive materials by irradiation with a high density electron beam. The majority of the soot in all samples was found as mixed particles with **sulfate-containing spherules** or as clusters of **such** spherules. For samples showing high enhancement (**>1.30**) of BC light absorption, TEM showed that the internally mixed soot-containing particles tended to have a more spherical shape and to be **thickly-coated**. The SP2 measurements also suggested that the proportion of thickly-coated soot was greater. Thus, the observed enhancement of BC light absorption was found to differ according to the mixing states and morphology of soot-containing particles. The enhancement of BC light absorption in our *in situ* measurements and its relation with individual features of soot-containing particles will be useful to evaluate direct radiative forcing in the **downwind** areas of large emission sources of BC.

## **1 Introduction**

Black carbon (BC) is contained in particles emitted from fossil fuel combustion and biomass/biofuel burning. It is known as a strong absorber of visible spectrum solar radiation in the atmosphere (e.g., Ramanathan and Carmichael, 2008; Bond et al., 2013). Similar to greenhouse gases, this absorption by BC is thought to lead to large positive radiative forcing; however, this assumption remains uncertain (IPCC, 2013). In the estimation of direct radiative forcing by BC particles, understanding how to treat the mixing state and optical properties of the BC and other materials are particularly important factors for reducing this uncertainty (Ma et al., 2012). **In relation to the global effect of BC, marked anthropogenic emissions of pollutants by recent economic development in eastern Asia is an important**

1 consideration (Streets et al., 2003; Ohara et al., 2007; Kurokawa et al., 2013). In addition to  
2 BC, precursor gases of secondary aerosol materials have been heavily emitted in eastern Asia  
3 (Bond et al., 2004; Kurokawa et al., 2013).

4 BC is **operationally** defined as a carbonaceous material with a deep black appearance caused  
5 by a significant imaginary portion of the refractive index. It roughly corresponds with  
6 elemental carbon (EC), which refers to the nonvolatile carbon present below a certain  
7 temperature (typically 550 °C) (Andreae and Gelencsér 2006, Bond and Bergstrom, 2006).  
8 Carbonaceous particles originating from fossil fuel combustion are observed as soot by  
9 electron microscope (e.g., Murr and Soto, 2005). Soot has an aggregation morphology of  
10 globules with a diameter of tens of nanometres that consist of concentrically wrapped  
11 graphitic layers (Pósfai et al., 2004; Murr and Soto, 2005). Although the definitions of soot  
12 and BC are different, they were considered equivalent for the purposes of this work. Soot  
13 particles that are freshly emitted by fossil fuel combustion are attached/coated with secondary  
14 aerosol materials, such as sulfate, nitrate, and organics, through atmospheric aging processes  
15 (Weingartner et al., 1997; Zuberi et al., 2005). Atmospheric aging processes of aerosol  
16 particles include adsorption and condensation of semi-volatile materials, coagulation of  
17 particles with other pre-existing aerosol particles, heterogeneous reactions at the particle  
18 surface with gaseous species, and cloud processing in the atmosphere (Fuchs, 1964; Husar  
19 and Whitby, 1973; Mamane and Gottlieb, 1989; Meng and Seinfeld, 1994; Ueda et al., 2014).  
20 Several studies using electron microscopy have reported that soot particles tend to be coated  
21 with large amounts of secondary materials in an aged air mass, whereas air masses in urban  
22 areas contain some **uncoated** soot particles (Pósfai et al., 1999; Hasegawa et al., 2002; Vester  
23 et al., 2007; Ueda et al., 2011; Adachi et al., 2014). **Ueda et al. (2011) reported that in leeward  
24 areas, soot-containing particles were internally mixed with the largely soluble materials in  
25 polluted air masses transported from eastern Asia. Moreover, a fraction of the soot-containing  
26 particles had an irregular shape due to mixing with clusters of spherical sulfate, that is,  
27 considered to be generated by coagulation processes under dry and high aerosol concentration  
28 conditions.**

29 The presence of coatings on BC particles is known to enhance the magnitude of light  
30 absorption by the BC particles, referred to as the “lensing effect”. The enhancement of light  
31 absorption by BC particles by coating ( $E_{\text{abs}}$ ) is expressed as the ratio of light absorption of  
32 coated BC particles to **uncoated** BC particles. Models often **apply a constant  $E_{\text{abs}}$  value or**

1 estimate  $E_{\text{abs}}$  assuming a core-shell (the BC core and coating materials) shaped spherical  
2 particle (Bond et al., 2013 and references therein). However, several studies have indicated  
3 that estimation assuming a core-shell structure with a clear shell tends to overestimate the  $E_{\text{abs}}$   
4 values (Lack and Cappa, 2010; Adachi et al., 2010). Lack and Cappa (2010) estimated  $E_{\text{abs}}$  of  
5 BC particles coated by brown carbon based on calculations using core-shell Mie theory. They  
6 showed that the lensing effect can be reduced from the non-absorbing coating case by up to  
7 25%–30% when averaged across the visible radiation spectrum. For Mexico City, Adachi et  
8 al. (2010) obtained three-dimensional shapes of soot-containing particles embedded in  
9 organic matter and sulfate using electron tomography with a **transmission electron microscope**  
10 **(TEM)**, and calculated the optical properties using a discrete dipole approximation. They  
11 reported that the core-shell model overestimated light absorption by ~30% compared to the  
12 model for irregularly shaped soot-containing particles.

13 Recently, the  $E_{\text{abs}}$  values have been measured by several studies based on *in situ* measurement  
14 of optical properties, using photoacoustic spectrometers (PAS) with a **thermodenuder (TD)**.  
15 **The reported  $E_{\text{abs}}$  values are from non-detectable to 1.43 in Toronto (Canada) (Knox et al.,**  
16 **2009, Chan et al., 2011, Healy et al., 2015), 1.38 in Boulder (USA) (Lack et al., 2012), 1.06 in**  
17 **California (USA) (Cappa et al., 2012), 1.10 (August) and non-detectable (January) in Nagoya**  
18 **(Japan) (Nakayama et al., 2014), and 1.4 at Detling (UK) (Liu et al., 2015). In these studies,**  
19  $E_{\text{abs}}$  was estimated as the ratio between absorption of ambient particles and particles heated in  
20 a **TD** to remove non-BC materials. **However, there have been very few observational studies**  
21 **reported the contributions of lensing effect and their relation with morphology of individual**  
22 **BC-containing particles in a well-aged air mass.**

23 To elucidate the enhancement of light absorption of aged BC particles **of Asian outflow** and  
24 their relation with the amount, morphology, and composition of coating materials, we  
25 conducted atmospheric observations of continental outflow at Noto Peninsula, Japan, in  
26 spring 2013. This atmospheric observation site has been previously used to study continental  
27 outflow (Maki et al., 2010; Iseki et al., 2010; Ishiyama et al., 2015). In the present study, the  
28 **absorption** and scattering coefficients of aerosol particles were directly measured using a 3 $\lambda$ -  
29 photoacoustic spectrometer (Droplet Measurement Technologies, PASS-3) with and without  
30 passage through a **TD**, and the contribution of the lensing effect was estimated. Specific  
31 attention was given to the relations between the enhancement of light absorption and the  
32 coating condition of individual soot-containing particles based on the TEM analysis.

1

## 2 **2 Field observation and laboratory analysis methods**

### 3 **2.1 Observation site and instrumentation**

4 Atmospheric observations were conducted at NOTO Ground-based Research Observatory  
5 (NOTOGRO) in Suzu City, Japan (37.5 °N, 137.4 °E), from April 17 to May 14, 2013. Suzu  
6 City is located on the north coast of Noto Peninsula. The physical and chemical parameters of  
7 aerosol particles and the concentrations of gaseous species have been continually monitored at  
8 the site. Ambient air was sampled through a PM10 inlet that was placed 14.7 m above the  
9 ground. Each measurement system was set in a room and connected to a flow-splitter  
10 downstream of the PM10 inlet. Chemical constituents of the aerosols were assessed using an  
11 aerosol chemical speciation monitor (Aerodyne Research, ACSM) capable of monitoring the  
12 bulk chemical components (organics,  $\text{NH}_4^+$ ,  $\text{SO}_4^{2-}$ ,  $\text{NO}_3^-$ , and  $\text{Cl}^-$ ) of non-refractory  
13 submicrometer-sized aerosols (NR-PM<sub>1</sub>). A PM<sub>2.5</sub> cyclone (with a cut off size of 2.5  $\mu\text{m}$  at a  
14 flow rate of 3 L min<sup>-1</sup>) was installed upstream of the ACSM inlet to remove coarse particles.  
15 The ionization efficiency of nitrate and the relative ionization efficiency of ammonium were  
16 determined by the standard calibration procedure (Ng et al., 2011) using  $\text{NH}_4\text{NO}_3$  (99.5%,  
17 Strem Chemicals). A collection efficiency (CE) of 0.3 was applied to the ACSM data. The  
18 value of CE was determined by comparing the mass concentrations of ammonium and sulfate  
19 derived by the ACSM to those measured by a conventional filter based off-line chemical  
20 analysis. The procedures to determine the CE value are described in the Supplemental  
21 Material (S1). It should be noted that selection of the CE value itself does not affect the  
22 discussion in this study, although the uncertainties in mass concentrations of NR components  
23 may be large (see section S1). Data for the chemical constituents were obtained every 30 min.  
24 During our observation period, more than 90% of the measured non-refractory materials were  
25  $\text{SO}_4^{2-}$ ,  $\text{NH}_4^+$ , and organics by mass. A particle size distribution between 8 and 346 nm in  
26 diameter was measured by a scanning mobility particle sizer (SMPS) (TSI, model 3936L76)  
27 placed downstream of the PM10 inlet. We set additional systems in the flow-splitter  
28 downstream of the PM10 inlet during this observation campaign, as shown in sections 2.2 and  
29 2.3.

30 The concentrations of  $\text{NO}_x$  and  $\text{NO}_y$  were measured using a  $\text{NO}-\text{O}_3$  chemiluminescence  
31 detector (Thermo Fisher Scientific, model 42i-TL) with a near-UV LED photolytic converter

1 and a molybdenum reduction catalyst (Mo converter) (Thermo Fisher Scientific, part No.  
2 9445) heated to 598 K, respectively. Detailed information for these measurements of NO<sub>x</sub>  
3 (Sadanaga et al., 2010) and NO<sub>y</sub> (Sadanaga et al., 2008; Yuba et al., 2010; 2014) have been  
4 given previously.

5

## 6 **2.2 *In situ* measurements of optical and physical properties of particles with** 7 **and without passage through the TD**

8 A schematic diagram of the experimental setup to measure the optical and physical properties  
9 of particles with or without passage through a TD is presented in Figure 1. Coarse aerosol  
10 particles were removed by a PM<sub>2.5</sub> cyclone (URG, URG-2000-30EH). After being dried by  
11 diffusion dryers with silica gel, the sample air was introduced alternately to a reference line  
12 and two TD lines to measure, respectively, ambient particles directly and after the evaporation  
13 of volatile materials under high temperature conditions. The same type of TDs used in our  
14 previous studies (Guo et al., 2014; Nakayama et al., 2014) was used in this study. The TD  
15 consists of a stainless tube (outer and inner diameters: 12.7 and 10.2 mm, respectively; length:  
16 600 mm) and electronic jacket heaters (Heater Engineer, P-series). Flow rates through the TD  
17 was 1.28 lpm, and the residence time for the sample aerosols in the TD was estimated to be  
18 2.3 s, on the assumption of plug flow conditions (at 20°C). The temperatures of the two TDs  
19 were maintained at 300 °C and 400 °C. The lines were switched every 10 min using two-way  
20 ball valves. Then, the sample air was introduced to the PASS-3, another SMPS (TSI, model  
21 3936L72), and a single-particle soot photometer (Droplet Measurement Technologies, SP2).  
22 The sampling flow rates of the PASS-3, SMPS, and SP2 were 1.0, 0.2, and 0.08 L min<sup>-1</sup>,  
23 respectively. The relative humidity in the cell of the PASS-3 was lower than 11% throughout  
24 the observation period.

25 The SMPS was used to measure the particle size distribution between 18 and 982 nm in  
26 diameter every 5 min. The SP2 was used to measure the mass concentration, size, and mixing  
27 state of single refractory BC (rBC) particles. The SP2 is based on the laser-induced  
28 incandescence (LII) method. The basic measurement principle of SP2 has been described  
29 previously (Gao et al., 2007; Moteki and Kondo, 2007). Before and after measurement,  
30 calibration of rBC was performed by measuring the LII signal intensities from size-specified  
31 fullerene particles (Alfa Aesar; stock 40971, lot L20W054) generated by an atomizer through

1 a differential mobility analyzer (DMA) (TSI, model 3080). The size of rBC was derived by  
2 assuming sphericity and a fixed density of  $1.8 \text{ g/cm}^3$ . The mixing state of rBC-containing  
3 particles was qualitatively estimated by the lag-time of the LII peak with respect to the peak  
4 of the scattering signal (Moteki and Kondo, 2007). Use of the SMPS in our measurement  
5 system was ended on 13 May, while use of the PASS-3 and SP2 was ended on 14 May.

6 The PASS-3 instrument was used to measure the absorption [ $b_{\text{abs}}(\lambda)$ ] and scattering [ $b_{\text{sca}}(\lambda)$ ]  
7 coefficients at 405, 532, and 781 nm. Details of the performance and calibration procedures of  
8 the PASS-3 have been described elsewhere (Nakayama et al., 2013, 2015). Note that the  
9 absolute values of the calibration factors do not influence to the  $E_{\text{abs}}$  values, which are used  
10 for discussion in the present study. The  $b_{\text{sca}}(532 \text{ nm})$  data were not used in this study because  
11 of a strong particle size dependence of the calibration factor at 532 nm (Nakayama et al.,  
12 2015). For background interpolation, measurements of filtered air were conducted using a  
13 particulate filter (Balston) for 3 min every 10 min. The influence of light absorption of  $\text{NO}_2$   
14 was found to be small ( $<0.05$  and  $<0.04 \text{ Mm}^{-1}$  at 405 and 532 nm, respectively) based on the  
15 estimation using transmittance of  $\text{NO}_2$  through filter and inlet tube as well as mixing ratio of  
16  $\text{NO}_2$ , and was taken into account for the determination of  $b_{\text{abs}}$  values. The 3-hour averaged  
17 values for each sampling line were estimated from six sets of 10 min data. By taking two  
18 standard deviations ( $2\sigma$ ) of each signal during the filtered air measurements, the typical  
19 detection limits for the 3-hour averaged data of  $b_{\text{abs}}$  (405 nm),  $b_{\text{abs}}$  (532 nm),  $b_{\text{abs}}$  (781 nm),  
20  $b_{\text{sca}}$  (405 nm), and  $b_{\text{sca}}$  (781 nm) were estimated to be 1.0, 1.9, 1.1, 0.7, and  $0.3 \text{ Mm}^{-1}$ ,  
21 respectively. Note that these detection limits varied depending on the magnitude of the drift in  
22 each signal.

23 In our system, particle loss and charring can occur in the TD lines. Using thermal/optical  
24 methods, some analytical studies of elemental and organic carbon in atmospheric particles  
25 reported that the degree of increase in light absorption of particles by charring differed among  
26 different organic material compositions (Yang and Yu, 2002; Yu et al., 2002). Based on the  
27 measurement of absorption at 680 nm wavelength under He induced conditions, Yang and Yu  
28 (2002) showed that charring of a sample including a large amount of water soluble organic  
29 carbon can increase from around  $400 \text{ }^\circ\text{C}$ . The charring effect can vary depending on the  
30 aerosol composition and, therefore, with time. In this observation, the ratios of the mass  
31 concentration of rBC measured by the SP2 without heating [ $m_{\text{rBC}}(25 \text{ }^\circ\text{C})$ ] to that after heating  
32 [ $m_{\text{rBC}}(T)$ ] ( $T = 300$  and  $400 \text{ }^\circ\text{C}$ ) varied depending on time with averages ( $\pm 1\sigma$ ) of  $1.08 \pm 0.28$

1 and  $1.03 \pm 0.30$  at 300 °C and 400 °C, respectively. Considering the estimated particle loss in  
2 our TD (~17% and ~20% at 300 and 400 °C, respectively (Guo et al. 2014)), our results  
3 suggest that non-negligible amount of rBC (10%–20% of ambient rBC) were formed in the  
4 TD, possibly due to charring by heating. In the present study, the  $E_{\text{abs}}$  values were estimated  
5 by taken these effects into account, assuming that light absorbing property of ambient rBC is  
6 same with that of rBC formed by heating in the TD and detected by the SP2,

$$7 \quad E_{\text{abs}}(\lambda, T) = \frac{b_{\text{abs}}(\lambda, 25\text{ °C})/b_{\text{abs}}(\lambda, T)}{m_{\text{rBC}}(25\text{ °C})/m_{\text{rBC}}(T)}, \quad (1)$$

8 where  $\lambda$  and  $T$  were measurement wavelength and TD temperature, respectively.

### 9 **2.3 Samples of individual particles and TEM analyses**

10 Aerosol particles were collected for morphological analysis using TEM (JEM-1400; JEOL).  
11 The sampling line for TEM analysis was placed downstream of the PM10 inlet. To analyze  
12 particles under the same conditions as PASS-3 and SP2, dried aerosols (after passage through  
13 diffusion dryers) were collected using a two-stage cascade impactor (50% cutoff aerodynamic  
14 diameters of the two stages were 1.5  $\mu\text{m}$  and 0.3  $\mu\text{m}$  at a flow rate of 0.7 L  $\text{min}^{-1}$ ) on carbon-  
15 coated nitrocellulose (collodion) films. In this study, samples from the second stage (50% cut  
16 off diameter of 0.3  $\mu\text{m}$ ) were analyzed. Aerosol samples were collected for 10–20 min.  
17 Typically, 1–2 samples were taken per day during the campaign. A fraction of the samples  
18 was collected after passing the particles through the same type of TDs used for the *in situ*  
19 measurements (section 2.2) maintained at 300 or 400 °C. The TEM samples were stored  
20 under dry conditions at room temperature until analyses. According to the  $b_{\text{abs}}$  values, the four  
21 samples obtained without passing the particles through the TD and one sample obtained after  
22 passing the particles through the TD maintained at 400 °C were selected and analyzed.

23 To obtain stereoscopic information of particles from 2-dimensional microphotograph,  
24 particles were coated with a Pt/Pd alloy at a shadowing angle of 26.6° (arctan 0.5), according  
25 to the method of Okada (1983). The Pt/Pd coating thickness was about 7 Å. The scanned  
26 image was processed using image analysis software (Win Roof; Mitani Corp.) to estimate the  
27 projected area of the particles. Elemental compositions of individual particles were analyzed  
28 using an energy-dispersive X-ray spectrometer (EDS) along with the TEM. The EDS was  
29 operated at an accelerating voltage of 120 kV. Elemental analyses were performed for C, Na,  
30 Mg, Al, Si, P, S, Cl, K, Ca, Ti, V, Cr, Mn, Fe, Ni, Zn, Sn, and Pb. The X-ray spectrum was

1 obtained using a detector with a counting time of 20 s per particle. The peak intensities of the  
2 elemental compositions in individual particles were quantified from the spectrum after  
3 deduction of the background spectrum near the particles. Based on the peak intensity,  
4 compositional particle types were classified as sulfate-rich, carbon-rich, sea salt-rich, aged sea  
5 salt-rich, crustal-rich, or others. Carbon-rich particles have the largest C peak. Sulfate-rich  
6 particles have the largest S peak and are absent of Na. Sea salt-rich particles have the largest  
7 Na peak or are Na-containing particles having the largest Cl peak. Aged sea salt-rich particles  
8 are Na-containing particles having the largest S peak. Crustal-rich particles have the largest  
9 peaks of Al, Si, or Fe. Particles having peaks other than those above, or not having a  
10 detectable peak, were classified as others. In this classification, a spectrum larger than two  
11 times the standard deviation of the background spectra, **which are spectra for non-particle**  
12 **areas measured between each sample analysis**, was used as the detectable spectrum of the  
13 particles to eliminate background noise effects. However, it should be noted that the standard  
14 deviation of the background C spectra is high because of the use of C-coated collodion film;  
15 therefore, there is a possibility that the number of C-rich particles is actually higher than that  
16 counted. To overcome this, the ratio of C to another element before elimination of the noise  
17 was utilized as an index of carbon content (Section 3.3.2).

18

### 19 **3 Results and discussion**

#### 20 **3.1 Temporal variation of optical properties**

21 Figure 2 shows the temporal variations in absorption [ $b_{\text{abs}}(\lambda)$ ] and scattering [ $b_{\text{sca}}(\lambda)$ ]  
22 coefficients and enhancement of light absorptions [ $E_{\text{abs}}(\lambda)$ ] observed during April 17–May 14,  
23 2013. Averages of  $b_{\text{abs}}(\lambda)$  and  $b_{\text{sca}}(\lambda)$  during the entire observation period are listed in Table 1.  
24 The  $b_{\text{abs}}(405 \text{ nm})$  and  $b_{\text{abs}}(781 \text{ nm})$  at 25 °C varied from close to 0 to 10  $\text{Mm}^{-1}$  and 0 to 5  $\text{Mm}^{-1}$ ,  
25 respectively. High  $b_{\text{abs}}(\lambda)$  events (higher than 5  $\text{Mm}^{-1}$  at 405 nm) were observed on April 19,  
26 22, and 27–29 and on May 6, 10, and 13–14. The  $b_{\text{sca}}$  at 25 °C was almost synchronous with  
27  $b_{\text{abs}}$ , but the values were about ten times larger (Table 1). For sample air that passed through  
28 the **TD** at 300 °C and 400 °C, averaged  $b_{\text{sca}}$  values were, respectively, one-seventh and one-  
29 eighth of those at 25 °C at 405 nm, and one-fourth of those at 25 °C at 781 nm (Figure 2b and  
30 d). In contrast, the values of  $b_{\text{abs}}(405 \text{ nm})$  and  $b_{\text{abs}}(781 \text{ nm})$  at high temperature (300 °C and  
31 400 °C) were only slightly different from those at 25 °C (Figure 2a and c).

1 **Most** of the  $E_{\text{abs}}(405 \text{ nm})$  values on April 19, 22–23, 26–29, and May 5–6 were less than 1.0  
2 and also less than the  $E_{\text{abs}}(532 \text{ nm})$  and  $E_{\text{abs}}(781 \text{ nm})$  values, **while** the  $E_{\text{abs}}(\lambda)$  values on May  
3 13–14 were greater than 1.0 at all wavelengths. Averaged  $E_{\text{abs}}(\lambda)$  for the data above the  
4 detection limit during the entire observation period are also listed in Table 1. Similar averaged  
5  $E_{\text{abs}}(\lambda)$  values between 300 °C and 400 °C were obtained at each wavelength. Because brown  
6 carbon is considered to absorb light only at shorter visible and UV wavelengths (Andreae and  
7 Gelencsér, 2006; Moosmüller et al., 2009),  $E_{\text{abs}}(405 \text{ nm})$  was expected to be larger than  
8  $E_{\text{abs}}(781 \text{ nm})$  if light absorption by organic materials evaporated at temperatures below 300 or  
9 400 °C contributed to the total light absorption at 405 nm. However, this study produced the  
10 opposite result. This can be explained by the increase of **“brownish materials”** by heating.  
11 **Here, the “brownish materials” are defined as the materials which were generated by heating**  
12 **in the TD and had significant light absorption at shorter visible wavelengths, to distinguish**  
13 **with ambient brown carbon particles.**

14 In this study, as explained in the previous section,  $b_{\text{abs}}(\lambda)$  was corrected for the effect of loss  
15 and formation of rBC inside the TDs using the mass concentration of rBC measured by SP2.  
16 However, the absorption by **brownish materials** that was potentially formed in the TDs might  
17 not be corrected accurately using this method because of the difference in wavelength  
18 dependence of light absorption between BC and **brownish materials**. According to the above  
19 explanation,  $E_{\text{abs}}(405 \text{ nm})$  and  $E_{\text{abs}}(532 \text{ nm})$  might have been particularly underestimated due  
20 to the absorption by **brownish materials** formed in the TDs. Because the influence of the  
21 formation of **brownish materials** on  $E_{\text{abs}}(781 \text{ nm})$  should be minimal,  $E_{\text{abs}}(781 \text{ nm})$  is  
22 considered to represent the lensing effect in later discussions.

23 **It should be noted that  $E_{\text{abs}}(781 \text{ nm})$  was calculated using eq (1) on the assumption that the**  
24 **light absorbing property of ambient rBC was same with that of rBC generated in the TD. If**  
25 **mass absorption cross section at 781 nm for rBC generated in the TD would be different by**  
26 **50% with that for ambient rBC, the lensing effect could be underestimated or overestimated**  
27 **by 0.05–0.10, considering 10%–20% of rBC were generated by heating in the TD (section**  
28 **2.2).**

### 29 **3.2 Relations between backward air mass trajectories and optical properties**

30 Figure 3 presents (a) the location of NOTOGRO, and (b–e) the 3 day backward air trajectories  
31 for air masses reaching the observation site. The backward trajectory data were computed

1 using the Hybrid Single-Particle Lagrangian Integrated Trajectory (HYSPLIT 4) model  
2 developed by the National Oceanic and Atmospheric Administration (NOAA) Air Resources  
3 Laboratory (ARL) (Draxler and Rolph, 2003; Rolph, 2003). The trajectories are colored  
4 according to  $b_{\text{abs}}$  (405 nm) and  $b_{\text{abs}}$  (781 nm), and to  $E_{\text{abs}}$ (405 nm) and  $E_{\text{abs}}$ (781 nm) calculated  
5 from  $b_{\text{abs}}$  values at 25 °C and 300 °C. The trajectories for  $E_{\text{abs}}$  calculated from  $b_{\text{abs}}$  data below  
6 the detection limit are presented as thin lines in Figures 3d and e.

7 The  $b_{\text{abs}}$  tended to be greater in air masses from the East Asian continent and lower in air  
8 masses from the north, such as from the Okhotsk Sea. When the greatest  $b_{\text{abs}}$  value was  
9 observed on the morning of May 14, the air mass originated from around Shanghai and was  
10 transported over the East China Sea. Large amounts of BC and precursors of secondary  
11 aerosols are considered to be emitted from the industrial areas facing the Yellow Sea and East  
12 China Sea in eastern China (Streets et al., 2003; Bond et al., 2004). Pollution events involving  
13 large amount of aerosols have been reported around the industrial areas in eastern China (Gao  
14 et al., 2009) and their leeward areas (Takami et al., 2005, 2007).

15 The  $E_{\text{abs}}$  at both 405 and 781 nm tended to differ according to the origin of the air mass: the  
16  $E_{\text{abs}}$  was high (1.3–1.4 at 405 nm and 1.3–1.5 at 781 nm) when air mass originated from  
17 around Shanghai and was transported over the East China Sea (May 13–14), and was low (<  
18 1.0 at 405 nm and 1.0–1.3 at 781 nm) when the air mass originated from northern China or  
19 Siberia and was transported over northern Korea peninsula and the sea of Japan (April 19, 22,  
20 27, and 28), or from the sea of Japan or a region of the main island of Japan (April 22 and 29  
21 and May 6 and 10). The  $E_{\text{abs}}$  values for the air mass from the Okhotsk Sea were not  
22 determined because the absorption coefficients were below the detection limit.

23

### 24 **3.3 TEM analyses**

#### 25 **3.3.1 Physicochemical properties of aerosols**

26 The four samples collected during high  $b_{\text{abs}}$  events in May were analyzed using TEM. The  
27 start times of the sampling are shown with the arrows A–D in Figure 2a. The details of the  
28 samples are listed in Table 2. For all samples, the average  $E_{\text{abs}}$ (405 nm) values were smaller  
29 than the average  $E_{\text{abs}}$ (781 nm) values by 0.1–0.4.

1 Ratio of  $\text{NO}_x$  to  $\text{NO}_y$  has been used as an indicator of photochemical age of air mass (e.g.,  
2 Cappa et al., 2012). The ratio for samples A, B, C, and D were 0.43, 0.67, 0.38, and 0.24,  
3 respectively. The results suggest that the plume ages for samples C and D are greater than  
4 those for samples A and B, although quantitative estimation of the plume age is difficult due  
5 to the possible contributions of wet and dry depositions of  $\text{NO}_y$ .

6 Figure 4 portrays the 72-hour horizontal backward trajectories of air parcels for samples A, B,  
7 C, and D, starting at 500 m above sea level at the NOTOGRO site. The trajectories for  
8 samples A and B showed that the air masses were transported slowly and reached the  
9 observation site over the north coast of the main island of Japan. The air masses for sample C  
10 were from northern China and were transported over the Korean Peninsula and the Sea of  
11 Japan, while those for sample D were from the Shanghai area and were transported over the  
12 East China Sea and the Sea of Japan within ~3 days. Combining these trajectories with the  
13 results of the ratios of  $\text{NO}_x$  to  $\text{NO}_y$ , indicates that samples A and B were likely affected by  
14 emissions from the main island of Japan, while samples C and D could be considered to be  
15 mainly affected by continental outflow.

16 For samples A, B, and D, 96%, 88%, and 97%, respectively, of the mass concentration of  
17 non-refractory materials measured by the ACSM consisted of  $\text{SO}_4^{2-}$ ,  $\text{NH}_4^+$ , and organics  
18 (Table 2). The organic mass ratio for samples A, B, and D were 62%, 62%, and 24%,  
19 respectively. The BC mass concentrations measured by SP2 were 4%, 3%, and 2% of the total  
20 submicron particle mass (sum of the mass concentrations of BC and non-refractory materials)  
21 for samples A, B, and D, respectively. The inlet line of the ACSM system was connected to a  
22 different line from 12:00 May 12 to 17:30 May 13, 2013, and the data for this period are not  
23 used in this study.

24 Figure 5 presents number-based size distributions at 25 °C, 300 °C, and 400 °C, and the cross  
25 sectional area- and volume-based size distributions at 25 °C of aerosol particles during  
26 samplings A–D, as measured by SMPS. Because use of the SMPS (TSI, model 3696L72)  
27 placed downstream of the heating system (shown in Figure 1) was ended on May 13, the 8–  
28 346 nm size distribution measured by another SMPS (TSI, model 3936L76) placed  
29 downstream of the PM10 inlet is used on May 14. Number-size distribution at 25 °C shows  
30 that number concentrations were higher in the < 100 nm fraction for samples A and B, but for  
31 samples C and D were higher in the > 100 nm fraction. The inlet line of the ACSM system  
32 was connected to a different line from 12:00 May 12 to 17:30 May 13, 2013, and the data for

1 this period are not used in this study. By passing the particle through the TD maintained at  
2 300 °C or 400 °C, the total particle number concentration decreased by one-fourth to one-half  
3 and the distribution had peaks in the < 100 nm fraction for samples A–C. In contrast, particles  
4 with diameters between 100 to 400 nm mainly contributed to the total cross-sectional area and  
5 volume of particles for all samples, and this is considered to contribute mainly to their optical  
6 properties.

7 Figure 6a presents the mass equivalent size distributions of rBC measured by SP2 for samples  
8 A–D together with their log-normal best-fitting curves. The peak diameters were around 200  
9 nm for all samples and were slightly larger for samples C and D compared to those for  
10 samples A and B. Figure 6b presents the normalized-count distribution of lag-time for rBC  
11 with a mass equivalent diameter of  $200 \pm 10$  nm. Unfortunately, the coating thickness of rBC  
12 could not be obtained directly by SP2 in this study because of a mechanical issue on a  
13 detector to determine absolute position of particles in the laser beam. Instead, the lag-time is  
14 treated as an index of the mixing states of rBC-containing particles because the scattering  
15 signal of the thicker-coated rBC core is detected before the incandescence signal from the  
16 rBC (Moteki and Kondo, 2007). The bimodal distribution of lag-time could be reasonably  
17 fitted by combination of two Gaussian functions. The lag-time value of the uncoated fullerene  
18 soot particle employed in the calibration was  $0.8 \pm 0.5$   $\mu$ s, indicating that uncoated BC  
19 particles also should be within this range. Therefore, lag-time peaks for rBC with a diameter  
20 of  $200 \pm 10$  nm in the range 0.6–1.0  $\mu$ s and 2.3–2.6  $\mu$ s in Figure 6b should be non/less-coated  
21 and thickly-coated, respectively. The fractions of thickly-coated rBC were 73%, 65%, 81%,  
22 and 88% for samples A, B, C, and D, respectively, while the peak lag-times of non/less-  
23 coated rBC and thickly-coated rBC were similar for all samples. The greater count fraction of  
24 thickly-coated BC for samples C and D compared to those for samples A and B was  
25 consistent with the expectation based on the trajectories of the air masses: samples C and D  
26 were considered to be influenced mainly by continental outflow and samples A and B were  
27 likely influenced by emissions from the main island of Japan.

28

### 29 **3.3.2 Morphological types and mixing states**

30 Figure 7 shows examples of electron microphotographs, at the same magnification, before and  
31 after EDS analysis of samples A and D. Most of the particles in all samples had a rounded

1 shape or were clustered into boll shapes. The round particles and spherical portions of  
2 clustered particles in sample A were smaller than those of sample D. Comparing particles  
3 before and after EDS, a large particle mass was evaporated or sublimated due to beam  
4 damage by the high density electron beam, while some chain-shaped residues (shown by  
5 black triangles in Figures 7a' and 7b'), which could be characterized as soot, were often  
6 found in the particles after EDS. In sample A, non-soot residues were also found in most  
7 particles after EDS. This non-soot residue mostly showed a weak contrast against the  
8 background collodion film, such as the materials shown by white triangles in Figure 7a'. A  
9 fraction of soot-like particles coexisted with the weakly contrasting residues. Particles of  
10 samples B and C resembled those of sample A and D, respectively.

11 According to the methods used by Ueda et al., (2011), the particles were classified into seven  
12 types based on their morphological features, as presented in Figure 8. The pie chart for each  
13 type (Figure 8) indicates the number fraction of particles for each compositional type based  
14 on EDS analysis. The number below the pie graph is the number of particles in each type.  
15 Detailed information on the classification and features of each morphological type and  
16 estimation of volume-equivalent diameter is described in the Supplemental Material (S2).

17 For type 2, 3, 4, and 5 particles, EDS analysis indicates that most were composed mainly of  
18 sulfate. However, some of them also contained carbon and sulfur, and the mixed ratio of  
19 carbon in the particle differed between particle types. The averaged peak intensity C to S ratio  
20 for sulfate-rich particles was 0.45, 0.13, 0.88, and 0.33 for types 2, 3, 4 and 5, respectively.  
21 This result suggests that coccoid sulfate (type 3) was less mixed with organic matter, while  
22 dome-like sulfate (type 4) was mixed with a larger amount of carbon.

23 The mixing states of particles were classified by comparing particle shape and morphology  
24 before and after irradiation by the high, densely-intense electron beam of the EDS analysis.  
25 Some materials, such as ammonium sulfate and sulfuric acid, evaporate or sublimate due to  
26 irradiation by the intense electron beam, whereas non-volatile materials, including soot, sea  
27 salt, and crustal particles, remain on the film after irradiation (e.g., Li et al., 2003, 2010;  
28 Pósfai et al., 2003; Adachi et al., 2014). The types of mixing states are shown in Figure 9.  
29 Detailed information on the classification of mixing states is described in the Supplemental  
30 Material (S3). Based on the EDS analysis, type *a* particles are composed mainly of carbon  
31 and silicate. Type *b* particles were mostly classified as sulfate-rich, sea salt-rich, or aged sea  
32 salt-rich. For the sulfate-rich type *b* particles, the C to S ratios in the peak intensities were

1 relatively high (0.99 on average), suggesting that they also contained a large amount of  
2 carbonaceous material. The majority of the type *c*, *d*, *e*, and *f* particles were classified as  
3 sulfate-rich particles. The averaged C to S ratios in the peak intensities for sulfate-rich  
4 particles were 0.40, 0.45, 0.71, and 0.10 for types *c*, *d*, *e*, and *f*, respectively; type *e* particles  
5 contained relatively large amounts of carbon, whereas type *f* particles were composed mostly  
6 of sulfate. Similar particles to those of type *e* were also found, and regarded as organics,  
7 during observation of the Chinese continental outflow (Li et al., 2013).

8 Figures 10a and b show size-segregated number proportions of the mixing states and  
9 morphological types of the particles in samples A–D on the basis of the classification in Figs.  
10 9 and 8, respectively. The mixing states had two patterns: (1) a combination of type *c* (mixed  
11 particles of soot and volatile) and type *e* (semi-volatile) particles, as found in samples A and  
12 B; and (2) a combination of type *c* and type *f* (volatile) particles, as found in samples C and D.  
13 Comparing with the chemical compositions measured by ACSM, the proportion of type *e*  
14 particles to type *f* particles was higher in samples collected when the mass ratio of organics  
15 was relatively high. This corresponded with the ratio of C to S by EDS analysis for type *e* and  
16 *f* particles. The number proportion of soot-containing particles (types *a* and *c*) was about  
17 10%–50% at each size range. Most soot was found as mixed particles with volatile materials.  
18 Morphological types of particles in all the samples (Figure 10b) were mainly of type 2  
19 (spherical) in the smaller size range and type 5 (clustered) in the larger size range. Compared  
20 to samples A and B, the fraction of type 2 particles tended to be higher for samples C and D  
21 (0.3–0.6  $\mu\text{m}$ ).

22 Relatively large spherical and clustered sulfate-rich particles were found in aged air masses  
23 (samples C and D), as discussed in section 3.3.1. Similar spherical and clustered sulfate-rich  
24 particles were simultaneously observed in the Asian outflow at Cape Hedo (Ueda et al., 2011).  
25 Using a simple numerical model and meteorological conditions along the backward  
26 trajectories, Ueda et al. (2011) demonstrated that the presence of clustered particles under dry  
27 conditions was explained by coagulation processes over several days in polluted conditions.  
28 In the present study, spherical particles were simultaneously observed with clustered particles.  
29 In addition, the relative humidity along the backward air mass trajectories, which were  
30 computed using the HYSPLIT model, was lower than the deliquescence humidity of  
31 ammonium sulfate (80%) for about 1 day for sample A and about 2 days for samples B, C,  
32 and D before arrival at the site. Therefore, clustered particles would have been formed by

1 coagulation of spherical particles under dry conditions. The differences of spherical particle  
2 (and spherical parts of clustered particle) sizes among samples A–D might be attributed to the  
3 different sources and/or aging processes through the condensation of gaseous molecules.

4 Figure 10c shows size-segregated number proportions of the morphological types of soot-  
5 containing particles (i.e., types *a* and *c*) before EDS analysis. Number proportions for soot-  
6 containing particles show a similar tendency to those for all particles in Figure 10b. This  
7 indicates that the morphology of a large portion of soot-containing particles reflected the  
8 shape of the coating materials, while a portion of the soot-containing particles has a soot-  
9 aggregated shape (type 1) in samples A and B. The presence of the non/less-coated soot  
10 particles in samples A and B is consistent with the results obtained by the SP2 (Figure 6).

11

### 12 **3.3.3 Internal mixing states and shape factors for soot-containing particles**

13 The controlling factors of the lensing effect of a soot-containing particle include coating  
14 thickness, morphology and position of the soot, and composition of the coating materials. In  
15 this study, the shape factors for soot-containing particles (i.e., types *a* and *c*) were estimated  
16 by electron micrograph before and after irradiation with a high, densely-intense electron beam.

17 Table 3 lists average and 25<sup>th</sup> and 75<sup>th</sup> percentile values of parameters of the soot-containing  
18 particles (number, particle and soot diameter ( $d_p$ ,  $d_s$ ), volume fraction and relative position of  
19 soot ( $VF_s$ ,  $RP$ ), circularity factor ( $CF$ ) and aspect ratio ( $AR$ )) for each sample. Details of  
20 image analysis and estimation of these parameters were described in the Supplemental  
21 Material (S4). The soot diameters  $d_s$  were 0.2–0.3 and 0.2–0.4  $\mu\text{m}$  for particles with  $d_p$  of  $\leq$   
22 0.6 and  $> 0.6$   $\mu\text{m}$ , respectively. The  $d_s$  values are roughly consistent with the diameter of rBC  
23 determined using SP2 (Figure 6a). The  $VF_s$  were 21%–50% and  $\sim 10\%$  for particles with  $d_p$  of  
24  $< 0.6$  and  $> 0.6$   $\mu\text{m}$ , respectively. The  $VF_s$  values indicate that a large portion of the soot-  
25 containing particles were mixed with other materials. Although no significant differences in  
26  $VF_s$  values among the samples were observed for particles with  $d_p$  of  $> 0.6$   $\mu\text{m}$ , the  $VF_s$  values  
27 for samples A and B were higher than those for samples C and D for particles with  $d_p$  of  $< 0.6$   
28  $\mu\text{m}$ , likely due to the presence of the non/less-coated soot particles in samples A and B (as  
29 discussed in section 3.3.2). Low values of  $VF_s$  were also reported by observational studies at  
30 background and remote sites: for example, the average values (8%–28%) of the soot volume  
31 fraction for 0.15–0.8  $\mu\text{m}$  particles at an urban background site in Mainz, Germany (Vester et

1 al., 2007) and median value (15%) of the soot volume fraction for 0.05–0.3  $\mu\text{m}$  particles in  
2 Mexico City (Adachi and Buseck, 2008) and median values ( $< 20\%$  for 0.2–0.4  $\mu\text{m}$  and  $<$   
3  $10\%$  for 0.4–0.7  $\mu\text{m}$ ) of the insoluble soot volume fraction in Cape Hedo (Ueda et al., 2011).

4 The *CF* and *AR* represent shape factors. The averaged *CF* and *AR* values of samples C and D  
5 were near 1 ( $CF > 0.80$  and  $AR < 1.3$ ) for all size ranges, suggesting that a large fraction of  
6 the particles were near-spherical. Small *CF* values ( $< 0.4$ ) were observed for particles with  $d_p$   
7 of  $> 0.6 \mu\text{m}$  in samples A and B, likely due to the clustered morphology of the larger soot-  
8 containing particles (type 5, in Figure 10c).

9 The *RP* is an indicator of soot position in the particle. The averaged *RP* values were 0.4–0.6  
10 and 0.6–0.9 for  $< 0.6$  and  $> 0.6 \mu\text{m}$  particles, respectively. These values indicate that most of  
11 the soot was inside the sphere-equivalent diameter but not at the center of the particle. Our  
12 averaged *RP* values were almost equal to the average values (0.54) of soot particle position  
13 for 0.05–0.3  $\mu\text{m}$  particles in Mexico City (Adachi et al., 2010). It should be noted that the *RP*  
14 value was estimated with reference to the sphere-equivalent diameter in our method.  
15 Therefore, the *RP* values for particles with an irregular shape can be less than 1 even if soot is  
16 attached/partly-embedded on/in other materials.

17 Internal mixing states of the soot-containing particles were also classified, directly from the  
18 microphotograph, into three types: type *a* (non/less coated soot), an attached/partly-embedded  
19 type, and a coated type (Table 4). Particles were classified to the attached/partly-embedded  
20 type if at least part of the soot in a type *c* particle was apparent in the microphotograph before  
21 EDS analysis; otherwise, the particle was classified as the coated type. For samples A and B,  
22 the number fraction of attached/partly-embedded soot was about 30% for  $< 0.6 \mu\text{m}$  particles  
23 and 60%–70% for  $> 0.6 \mu\text{m}$  particles. For samples C and D, most of the soot ( $> 83\%$ ) was  
24 classified as the coated type. Soot-containing particles in samples A and B had more irregular  
25 shapes than those in samples C and D, although no clear difference in averaged *RP* values  
26 among the samples was found. These results suggested that the soot in samples A and B  
27 would not be thickly coated compared to that in samples C and D. Several observational  
28 studies of soot-containing particles using microscopy also found some attached/partly-  
29 embedded soot on/in sulfate-rich particles (Jonson et al., 2005; Shi et al., 2008; Adachi and  
30 Buseck, 2013).

31

### 3.4 Comparison of optical properties with mixing states and morphological features

As mentioned in Section 3.1, the  $E_{\text{abs}}$  values tended to be smaller at shorter wavelengths, possibly due to the formation of brownish materials in the TDs maintained at 300 °C or 400 °C. In this study, several samples for morphological analysis were collected after passing the particles through the TD maintained at 400 °C. Figure 12 shows an example electron micrograph of such particles. These were sampled just after the collection of sample A on May 6 when a small  $E_{\text{abs}}(405 \text{ nm})$  value (0.88) was observed (Table 2). Based on EDS analysis, some carbon-rich particles were found. The morphologies of the carbon-rich particles not only had a chain-like shape but were also spherical. These particles were not evaporated during irradiation by the high density electron beam of the EDS analysis. The spherical particle features (*i.e.*, non-volatile, spherical, and carbon-rich) were similar to tar ball, which is originated in biomass burning (Pósfai et al., 2003, 2004; Alexander et al., 2008; Adachi and Buseck, 2011). Alexander et al. (2008) quantified the optical properties of similar amorphous carbon sphere particles in the East Asian-Pacific outflow using the electron energy-loss spectrum in TEM, and indicated that these particles have strong light absorption, with mean refractive indices of  $1.67-0.27i$  at 550 nm. Although these carbon-rich, spherical, non-volatile particles were rare in our samples collected without passing the particles through the TD, a large number of particles in samples A and B had non-volatile residues after EDS analysis (type *e*, in Figure 10a). Therefore, the spherical, carbon-rich particles might be formed by heating, probably due to the incomplete charring of organic compounds, and could be brown in colour.

In contrast, the formation of brownish materials was not observed in our previous study at an urban area in Nagoya, although the same procedure was used to determine the wavelength dependent  $E_{\text{abs}}$  values (Nakayama et al., 2014). During the observations at Nagoya in August, most of the heated particles were found to be non-spherical (based on the effective density distribution measurements (Nakayama et al., 2014)). Differences in the source and degree of aging of carbonaceous particles may contribute to the observed difference in the wavelength dependence of  $E_{\text{abs}}$ . Our results suggest that attention needs to be paid when a TD is used to estimate the contributions of the lensing effect and brown carbon, especially for particles in aged air masses.

1 In this study, to avoid the possible contributions of the formation of brownish particles in the  
2 TD,  $E_{\text{abs}}(781 \text{ nm})$  is used for discussion of the lensing effect. The average  $E_{\text{abs}}(781 \text{ nm})$  values  
3 observed in this study (1.22 and 1.23 at 300 and 400 °C, respectively, Table 1) was larger  
4 than the values reported by Cappa et al. (2012) around large cities in California during early  
5 summer (on average 1.06 at 532 nm) and by Nakayama et al. (2014) in an urban area at  
6 Nagoya, Japan during August (on average 1.10 at 781 nm), likely because relatively aged  
7 particles were observed in this study. Very recently, Liu et al. (2015) reported the average  
8  $E_{\text{abs}}(781 \text{ nm})$  of 1.4 for BC particles emitted from fossil fuel and residential burning sources  
9 in winter at a rural site, Detling (45 km away from London) in UK. The average  $E_{\text{abs}}(781 \text{ nm})$   
10 value obtained in the present study is slightly lower than the value reported by Liu et al.  
11 (2015).

12 Most of the soot-containing particles in all the samples under high absorption coefficient  
13 conditions were internally-mixed with a large amount (> 50% of particle volume) of other  
14 materials (Table 3). Previous models based on Mie theory and assuming a core-shell (the BC  
15 core and coating materials) shape suggested  $E_{\text{abs}}$  values larger than 1.5 when particles had a  
16 heavy coating (Bond et al., 2006). The average  $E_{\text{abs}}$  value observed in this study was still  
17 smaller than the estimation assuming core-shell morphology. Adachi et al. (2010) estimated  
18 the lensing effect of irregularly shaped particles and those with an assumed core-shell shape,  
19 and reported that the difference in the calculated absorption was related to the position of soot  
20 in the particle and the fractal dimension. Based on their results, absorption of soot-containing  
21 particles with our averaged  $RP$  values (0.4–0.9) could be about 10%–25% smaller than the  
22 value estimated assuming core-shell morphology. The position of soot in the particle may  
23 contribute to the difference between observation and estimation, as previously suggested by  
24 Cappa et al. (2012).

25 Comparing among pollution events in this study, the  $E_{\text{abs}}(781 \text{ nm})$  values for the long range  
26 transported continental outflow (May 13 and 14) were larger (> 1.3) than those for the air  
27 masses likely affected by emissions from the main island of Japan (May 6 and 10), as listed in  
28 Table 2. These results are consistent with the results of the SP2 and TEM analyses. Greater  
29 count fractions of thickly-coated BC were observed in the SP2 measurements (Figure 6), and  
30 a greater number fraction of coated soot particles (Table 3) and lower volume fraction of soot  
31 in smaller particles (< 0.6  $\mu\text{m}$ ) (Table 4) were observed in samples C and D compared to  
32 samples A and B. In addition, number fractions of coated soot particles were greater during

1 the high  $E_{\text{abs}}$  events (samples C and D) compared to samples A and B (Table 5). The greater  
2 circularity of the soot-containing particles in samples C and D (Table 4, Figure 10c) may also  
3 contribute to the greater  $E_{\text{abs}}$  values, as discussed by Adachi et al. (2010). Although most soot-  
4 containing particles in all samples in this study were internally mixed with sulfate and  
5 organics, the number fraction of thickly-coated soot was higher in more aged air masses from  
6 China. Our results indicate that, according to the transport pathway and aging levels of the air  
7 mass, the magnitude of the lensing effect could change with changes in the mixing states and  
8 morphology of soot-containing particles.

9

#### 10 **4 Summary and Conclusions**

11 To elucidate the lensing effect of aged BC particles and their relation with the mixing state  
12 and morphology of individual particles, *in situ* measurements of the optical and chemical  
13 properties and size distributions of aerosols and the mixing state of rBC, as well as sampling  
14 for TEM analysis, were conducted at an Asian outflow site in Noto Peninsula, Japan, in spring  
15 2013.

16 The enhancement factor,  $E_{\text{abs}}(\lambda)$ , at 405, 532, and 781 nm was determined by comparing the  
17 light absorption of aerosol particles with and without passing through a TD maintained at  
18 300 °C or 400 °C. The  $E_{\text{abs}}$  values tended to be lower at shorter wavelengths. In samples  
19 exhibiting a relatively small enhancement of light absorption at 405 nm after passage of the  
20 particles through the TD (samples A and B), spherical, carbon-rich particles were found,  
21 implying that the brownish materials may be formed during the heating processes.

22 The  $E_{\text{abs}}(781 \text{ nm})$  values estimated using the data at the TD temperature of 300 °C, which was  
23 assumed to represent the magnitude of the lensing effect, was 1.22 on average. Large  $E_{\text{abs}}(781$   
24 nm) values ( $> 1.3$ ) were observed on May 13–14 when the air mass was transported over 2–3  
25 days from urban areas in China. In the samples collected on May 13–14 (samples C and D),  
26 most soot-containing particles were internally mixed with a large amount of coating materials  
27 involving sulfate. Results of SP2 measurement and TEM analyses indicated that the number  
28 proportion of thickly-coated soot particles tended to be greater in these air masses. In addition,  
29 most soot-containing particles in samples C and D were close to a spherical shape, whereas  
30 larger number fractions of soot-containing particles were mixed with cluster of sulfate  
31 containing spherules in samples A and B. These results suggest that the mixing state and

1 morphological features of soot-containing particles would be factors controlling the lensing  
2 effect of BC in this study. The relation between the magnitude of the lensing effect and the  
3 mixing state and morphology of individual soot-containing particles for well-aged air masses  
4 will be useful to evaluate the direct radiative forcing of aerosols, particularly in leeward areas  
5 of large emission sources of BC.

6

## 7 **Acknowledgements**

8 We express our gratitude to Ms. M. Sawano, Ms. S. Kagami (Kanazawa Univ.), and Mr. T.  
9 Yamasaki (Nagoya Univ.) for assisting our research. We gratefully acknowledge the NOAA  
10 Air Resources Laboratory (ARL) for providing the HYSPLIT transport model  
11 (<http://www.arl.noaa.gov/ready.html>). This work was performed with the support of the  
12 Grant-in-Aid for Scientific Research (KAKENHI 25701001 and 25740013) and Green  
13 Network of Excellence, Environmental Information (GRENE-ei) program from the Ministry  
14 of Education, Culture, Sports, Science and Technology (MEXT), the Global Environment  
15 Research Fund (2-1403) of the Ministry of the Environment, Japan, Toyoaki Scholarship  
16 Foundation, and the joint research program of the Solar-Terrestrial Environment Laboratory,  
17 Nagoya University.  
18

## 1 **References**

- 2 Adachi, K. and Buseck, P. R.: Internally mixed soot, sulfates, and organic matter in aerosol  
3 particles from Mexico City, *Atmos. Chem. Phys.*, 8, 6469–6481, doi:10.5194/acp-8-6469-  
4 2008, 2008.
- 5 Adachi, K. and Buseck, P. R.: Atmospheric tar balls from biomass burning in Mexico, *J.*  
6 *Geophys. Res. Atmos.*, 116, D5, doi: 10.1029/2010JD015102 , 2011.
- 7 Adachi, K. and Buseck, P. R.: Changes of ns-soot mixing states and shapes in an urban area  
8 during CalNex, *J. Geophys. Res. Atmos.*, 118, 3723–3730, doi: 10.1002/jgrd.50321, 2013.
- 9 Adachi, K., Chung, S. H., and Buseck, P. R.: Shapes of soot aerosol particles and implications  
10 for their effects on climate, *J. Geophys. Res.*, 115, D15206, doi:10.1029/2009JD012868, 2010.
- 11 Adachi, K., Zaizen, Y., Kajino, M., and Igarashi, Y.: Mixing state of regionally transported  
12 soot particles and the coating effect on their size and shape at a mountain site in Japan, *J.*  
13 *Geophys. Res. Atmos.*, 119, 5386–5396, doi: 10.1002/2013JD020880, 2014.
- 14 Alexander, D. T. L., Crozier, P. A., and Anderson, J. R.: Brown carbon spheres in East Asian  
15 outflow and their optical properties, *Science*, 321, 833–836, doi: 10.1126/science.1155296,  
16 2008.
- 17 Andreae, M. O. and Gelencs , A.: Black carbon or brown carbon? The nature of light-  
18 absorbing carbonaceous aerosols, *Atmos. Chem. Phys.*, 6, 3131–3148, 2006.
- 19 Bond, T. C., and Bergstrom, R. W.: Light absorption by carbonaceous particles: An  
20 investigative review, *Aerosol Sci. Tech.*, 40, 27–67, doi: 10.1080/02786820500421521, 2006.
- 21 Bond, T. C., Streets, D. G., Yarber, K. F., Nelson, S. M., Woo, J.-H., and Klimont, Z.: A  
22 technology-based global inventory of black and organic carbon emissions from combustion, *J.*  
23 *Geophys. Res.*, 109, D14203, doi: 10.1029/2003JD003697, 2004.
- 24 Bond, T. C., Habib, G., and Bergstrom, R. W.: Limitations in the enhancement of visible light  
25 absorption due to mixing state, *J. Geophys. Res.*, 111, D20211, doi:10.1029/2006JD007315,  
26 2006.
- 27 Bond, T. C., Doherty, S. J., Fahey, D. W., Forster, P. M., Berntsen, T., DeAngelo, B. J.,  
28 Flanner, M. G., Ghan, S., K rcher, B., Koch, D. Kinne, S., Kondo, Y., Quinn, P. K., Sarofim,  
29 M. C., Schultz, M. G., Schulz, M., Venkataraman, C., Zhang, H., Zhang, S., Bellouin, N.,

1 Guttikunda, S. K., Hopke, P. K., Jacobson, M. Z., Kaiser, J. W., Klimont, Z., Lohmann, U.,  
2 Schwarz, J. P., Shindell, D., Storelvmo, T., Warren, S. G., and Zender, C. S.: Bounding the  
3 role of black carbon in the climate system: A scientific assessment, *J. Geophys. Res. Atmos.*,  
4 118, 5380–5552, doi: 10.1002/jgrd.50171, 2013.

5 Cappa, C. D., Onasch, T. B., Massoli, P., Worsnop, D. R., Bates, T. S., Cross, E. S.,  
6 Davidovits, P., Hakala, J., Hayden, K. L., Jobson, B. T., Kolesar, K. R., Lack, D. A., Lerner,  
7 B. M., Li, S. M., Mellon, D., Nuaaman, I., Olfert, J. S., Petaja, T., Quinn, P. K., Song, C.,  
8 Subramanian, R., Williams, E. J., and Zaveri, R. A.: Radiative absorption enhancements due  
9 to the mixing state of atmospheric black carbon, *Science*, 337, 1078–1081,  
10 doi:10.1126/science.1223447, 2012.

11 Chan, T. W., Brook, J. R., Smallwood, G. J., and Lu, G.: Time-resolved measurements of  
12 black carbon light absorption enhancement in urban and near-urban locations of southern  
13 Ontario, Canada, *Atmos. Chem. Phys.*, 11, 10407-10432, doi:10.5194/acp-11-10407-2011,  
14 2011.

15 Draxler, R. R. and Rolph, G. D., 2003. HYSPLIT (HYbrid Single-Particle Lagrangian  
16 Integrated Trajectory) Model access via NOAA ARL READY Website, available at:  
17 <http://www.arl.noaa.gov/ready/hysplit4.htm> (last access: October 3, 2013), NOAA Air  
18 Resources Laboratory, Silver Spring, MD.

19 Fuchs, N.A.: The coagulation of aerosols, in *The mechanics of aerosols*, pp. 288–322, Dover  
20 Publications, Inc., New York, 1964.

21 Gao, R. S., Schwarz, J. P., Kelly, K. K., Fahey, D. W., Watts, L. A., Thompson, T. L.,  
22 Spackman, J. R., Slowik, J. G., Cross, E. S., Han, J. H., Davidovits, P., Onasch, T. B., and  
23 Worsnop, D. R.: A novel method for estimating light-scattering properties of soot aerosols  
24 using a modified single-particle soot photometer, *Aerosol Sci. Tech.*, 41, 125–135,  
25 doi:10.1080/02786820601118398, 2007.

26 Guo, X., Nakayama a, T., Yamada, H., Inomata, S., Tonokura, K., and Matsumi, Y.:  
27 Measurement of the light absorbing properties of diesel exhaust particles using a three-  
28 wavelength photoacoustic spectrometer, *Atmos. Environ.*, 94, 428–437,  
29 doi:10.1016/j.atmosenv.2014.05.042, 2014.

1 Hasegawa, S. and Ohta, S.: Some measurements of the mixing state of soot-containing  
2 particle at urban and non-urban sites, *Atmos. Environ.*, 36, 3899–3908, doi:10.1016/S1352-  
3 2310(02)00343-6, 2002.

4 Healy, R. M., Wang, J. M., Jeong, C.-H., Lee, A. K. Y., Willis, M. D., Jaroudi, E.,  
5 Zimmerman, N., Hilker, N., Murphy, M., Eckhardt, S., Stohl, A., Abbatt, J. P. D., Wenger, J.  
6 C., and Evans, G. J., Light-absorbing properties of ambient black carbon and brown carbon  
7 from fossil fuel and biomass burning sources, *J. Geophys. Res. Atmos.*, 120, 6619-6633,  
8 doi:10.1002/2015JD023382, 2015.

9 Husar, R.B. and Whitby, K.T.: Growth Mechanisms and size spectra of photochemical  
10 aerosols. *Environ. Sci. Tech.* 7, 241–247, doi: 10.1021/es60075a003, 1973.

11 Intergovernmental Panel on Climate Change (IPCC), *Climate Change 2013: The Physical*  
12 *Science Basis*, Cambridge Univ. Press, Cambridge, UK., 2013.

13 Iseki, S., Sadanaga, Y., Matsuki, A., Iwasaka, Y., Sato, K., Takenaka, N., and Bandow H.:  
14 Analyses of the concentration variations of ozone and carbon monoxide at Suzu, the Noto  
15 Peninsula, *J. Jpn. Soc. Atmos. Environ.*, 45, 256–263, doi: 10.11298/taiki.45.256, 2010. (in  
16 Japanese)

17 Ishiyama, A., Takaji, R., Sadanaga, Y., Matsuki, A., Sato, K., Osada, K., and Bandow, H.:  
18 Seasonal variations of peroxyacyl nitrates and alkyl nitrates concentrations at Suzu, the Noto  
19 Peninsula, *J. Jpn. Soc. Atmos. Environ.*, 50, 16-26, 2015. (in Japanese)

20 Johnson, K. S., Zuberi, B, Molina, L. T., Molina, M. J., Iedema, M. J., Cowin, J. P., Gaspar,  
21 D. J., Wang, C., and Laskin, A.: Processing of soot in an urban environment: case study from  
22 the Mexico City Metropolitan Area, *Atmos. Chem. Phys.*, 5, 3033–3043, doi:10.5194/acp-5-  
23 3033-2005, 2005.

24 Knox, A., Evans, G. J., Brook, J. R., Yao, X., Jeong, C.-H., Godri, K. J., Sabaliauskas, K., and  
25 Slowik, J. G.: Mass absorption cross-section of ambient black carbon aerosol in relation to  
26 chemical age, *Aerosol Sci. Technol.*, 43, 522–532, doi:10.1080/02786820902777207., 2009.

27 Kurokawa, J., Ohara, T., Morikawa, T., Hanayama, S., Greet, J.-M., Fukui, T., Kawashima,  
28 K., and Akimoto, H.: Emissions of air pollutants and greenhouse gases over Asian regions  
29 during 2000–2008: Regional Emission inventory in ASia (REAS) version 2, *Atmos. Chem.*  
30 *Phys.*, 13, 11019–11058, doi:10.5194/acp-13-11019-2013, 2013.

- 1 Ma, X., Yu, F., and Luo, G.: Aerosol direct radiative forcing based on GEOS-Chem-APM and  
2 uncertainties, *Atmos. Chem. Phys.*, 12, 5563–5581, doi:10.5194/acp-12-5563-2012, 2012.
- 3 Lack, D. A. and Cappa, C. D.: Impact of brown and clear carbon on light absorption  
4 enhancement, single scatter albedo and absorption wavelength dependence of black carbon,  
5 *Atmos. Chem. Phys.*, 10, 4207–4220, doi:10.5194/acp-10-4207-2010, 2010.
- 6 Lack, D. A., Langridge, J. M., Bahreini, R., Cappa, C. D., Middlebrook, A. M., and Schwarz,  
7 J. P.: Brown carbon and internal mixing in biomass burning particles, *Proc. Natl. Acad. Sci.*  
8 *USA*, 109, 14802–14807, doi: 10.1073/pnas.1206575109, 2012.
- 9 Li, J., Pósfai, M., Hobbs, P. V., and Buseck, P. R.: Individual aerosol particles from biomass  
10 burning in southern Africa: 2, Compositions and aging of inorganic particles, *J. Geophys.*  
11 *Res.*, 108, D13, 8484, doi:10.1029/2002JD002310, 2003.
- 12 Li, W. J., Shao, L. Y., and Buseck, P. R.: Haze types in Beijing and the influence of  
13 agricultural biomass burning, *Atmos. Chem. Phys.*, 10, 8119–8130, doi:10.5194/acp-10-8119-  
14 2010, 2010.
- 15 Li, W., Wand, T., Zhou, S., Lee, S. C., Huang, Y., Gao, Y., and Wang, W.: Microscopic  
16 observation of metal-containing particles from Chinese continental outflow observed from a  
17 Non-Industrial Site, *Environ. Sci. Tech.*, 4, 9124–9131, doi: 10.1021/es400109q, 2013.
- 18 Liu, S. Aiken, A. C., Gorkowski, K., Dubey, M. K., Cappa, C. D., Williams, L. R., Herndon,  
19 S. C., Massoli, P., Fortner, E. C., Chhabra, P. S., Brooks, W. A., Onasch, T. B., Jayne, J. T.,  
20 Worsnop, D. R., China, S., Sharma, N., Mazzoleni, C., Xu, L., Ng, N. L., Liu, D., Allan, J. D.,  
21 Lee, J. D., Fleming, Z. L., Mohr, C., Zotter, P., Szidat, S., and Prévôt, A. S. H., Enhanced  
22 light absorption by mixed source black and brown carbon particles in UK winter, *Nature*  
23 *Comm.*, 6, 8435, doi:10.1038/ncomms9435, 2015.
- 24 Ma, X., Yu, F., and Luo, G.: Aerosol direct radiative forcing based on GEOS-Chem-APM and  
25 uncertainties, *Atmos. Chem. Phys.*, 12, 5563–5581, doi:10.5194/acp-12-5563-2012, 2012.
- 26 Maki, T., Susuki, S., Kobayashi, F., Kakikawa, M., Tobo, Y., Yamada, M., Higashi, T.,  
27 Matsuki, A., Hong, C., Hasegawa, H., and Iwasaka, Y.: Phylogenetic analysis of atmospheric  
28 halotolerant bacterial communities at high altitude in an Asian dust (KOSA) arrival region,  
29 Suzu City, *Sci. Total Environ.*, 408, 4556–4562, doi:10.1016/j.scitotenv.2010.04.002, 2010.

1 Mamane, Y. and Gottlieb, J.: The study of heterogeneous reactions of carbonaceous particles  
2 with sulfur and nitrogen oxides using single particles. *J. Aerosol. Sci.* 20, 575–584,  
3 doi:10.1016/0021-8502(89)90104-3, 1989.

4 Meng, Z. and Seinfeld, J.H.: On the source of submicrometer droplet mode of urban and  
5 regional aerosols. *Aerosol Sci. Tech.*, 20, 253–265.1994.

6 Moosmüller, H., Chakrabarty, R. K., and Arnott, W. P.: Aerosol light absorption and  
7 its measurement: A review, *J. Quant. Spectrosc. Radiat. Transfer*, 110, 844–878,  
8 doi:10.1016/j.jqsrt.2009.02.035, 2009.

9 Moteki, N. and Kondo, Y.: Effects of Mixing State on Black Carbon Measurements by  
10 Laser-Induced Incandescence, *Aerosol Sci. Tech.*, 41, 398–417, doi:  
11 10.1080/02786820701199728, 2007.

12 Murr, L. E. and Soto, K. F.: A TEM study of soot, carbon nanotubes, and related fullerene  
13 nanopholyhedra in common fuel-gas combustion sources, *Mater. Charact.*, 55, 50–65. 2005.

14 Nakayama, T., Sato, K., Matsumi, Y., Imamura, T., Yamazaki, A., and Uchiyama, A.:  
15 Wavelength and NO<sub>x</sub> dependent complex refractive index of SOAs generated from the  
16 photooxidation of toluene, *Atmos. Chem. Phys.*, 13, 531–545, doi:10.5194/acp-13-531-2013,  
17 2013.

18 Nakayama, T., Ikeda, Y., Sawada, Y., Setoguchi, Y., Ogawa, S., Kawana, K., Mochida, M.,  
19 Ikemori, F., Matsumoto, K., and Matsumi, Y.: Properties of light-absorbing aerosols in the  
20 Nagoya urban area, Japan, in August 2011 and January 2012: Contributions of brown carbon  
21 and lensing effect, *J. Geophys. Res. Atmos.*, 119, 12721–12739, doi:10.1002/2014JD021744,  
22 2014.

23 Nakayama, T., Suzuki, H., Kagaminani, S., Ikeda, Y., Uchiyama, A., and Matsumi, Y.:  
24 Characterization of a three wavelength photoacoustic soot spectrometer (PASS-3) and a  
25 photoacoustic extinciometer (PAX), *J. Meteorol. Soc. Jpn.*, 93, 285-308,  
26 doi:10.2151/jmsj.2015-016, 2015.

27 Ng , N. L., Herndon, S. C., Trimborn, A., Canagaratna, M. R., Croteau, P. L., Onasch, T. B.,  
28 Sueper, D., Worsnop, D. R., Zhang, Q., Sun, Y. L., and Jayne, J. T.: An Aerosol Chemical  
29 Speciation Monitor (ACSM) for Routine Monitoring of the Composition and Mass  
30 Concentrations of Ambient Aerosol, *Aerosol Sci. Tech.*, 45, 780–794, doi:  
31 10.1080/02786826.2011.560211, 2011

1 Okada, K.: Nature of individual hygroscopic particles in the urban atmosphere. *J. Meteor. Soc.*  
2 *Japan*, 61, 727–735, 1983.

3 Ohara, T., Akimoto, H., Kurokawa, J., Horii, N., Yamaji, K., Yan, X., and Hayasaka, T.: An  
4 Asian emission inventory of anthropogenic emission sources for the period 1980–2020,  
5 *Atmos. Chem. Phys.*, 7, 4419–4444, doi:10.5194/acp-7-4419-2007, 2007.

6 Pósfai, M., Anderson, J. R., and Buseck, P. R.: Soot and sulfate aerosol particles in the remote  
7 marine troposphere, *J. Geophys. Res.*, 104, D17, 685–693, doi: 10.1029/1999JD900208, 1999.

8 Pósfai, M., R. Simonics, Li, J., Hobbs, P. V., and Buseck, P. R.: Individual aerosol particles  
9 from biomass burning in southern Africa: 1. Compositions and size distributions of  
10 carbonaceous particles, *J. Geophys. Res.*, 108, D13, doi:10.1029/2002JD002291, 2003.

11 Pósfai, M., Gelencser, A., Simonics, R., Arato, K., Li, J., Hobbs, P. V., and Buseck, P. R.:  
12 Atmospheric tar balls: Particles from biomass and biofuel burning, *J. Geophys. Res.*, 109,  
13 D06213, doi: 10.1029/2003JD004169, 2004.

14 Ramanathan, V. and Carmichael, G.: Global and regional climate changes due to black carbon,  
15 *Nature Geoscience*, 1, 221–227, doi:10.1038/ngeo156, 2008.

16 Rolph, G. D., 2003. Real-time environment applications and display system (READY),  
17 NOAA Air Resour. Lab., Silver Spring, Md., Available at:  
18 <http://www.arl.noaa.gov/ready/hysplit4.html> (last access: October 3, 2013)

19 Sadanaga, Y., Yuba, A., Kawakami, J., Takenaka, N., Yamamoto, M., and Bandow, H.: A  
20 gaseous nitric acid analyzer for the remote atmosphere based on the scrubber difference/NO-  
21 ozone chemiluminescence method, *Anal. Sci.*, 24, 967–971, doi: 10.2116/analsci.24.967,  
22 2008.

23 Sadanaga, Y., Fukumori, Y., Kobashi, T., Nagata, M., Takenaka, N., and Bandow, H.:  
24 Development of a selective light-emitting diode photolytic NO<sub>2</sub> converter for continuously  
25 measuring NO<sub>2</sub> in the atmosphere, *Anal. Chem.*, 82, 9234-9239, doi:10.1021/ac101703z,  
26 2010.

27 Shi, Z., Zhang, D., Ji, H., Hasegawa, S., and Hayashi, M.: Modification of soot by volatile  
28 species in an urban atmosphere, *Sci. Total, Environ.*, 389, 195 –201,  
29 doi:10.1016/j.scitotenv.2007.08.016, 2008.

1 Streets, D.G., Bond, T. C., Carmichael, G. R., Fernandes, S. D., Fu, Q., He, D., Klimont, Z.,  
2 Nelson, S. M., Tsai, N. Y., Wang, M. Q., Woo, J.-H., and Yarber, K. F.: An inventory of  
3 gaseous and primary aerosol emissions in Asia in 2000, *J. Geophys. Res.*, 108, D21,  
4 doi:10.1029/2002JD003093, 2003.

5 Takami, A., Miyoshi, T., Shimono, A., and Hatakeyama, S. : Chemical composition of fine  
6 aerosol measured by AMS at Fukue Island, Japan during APEX period, *Atmos. Environ.*, 39,  
7 4913–4924, doi:10.1016/j.atmosenv.2005.04.038, 2005.

8 Takami, A., Miyoshi, T., Shimono, A., Kaneyasu, N., Kato, S., Kajii, Y., and Hatakeyama,  
9 S. : Transport of anthropogenic aerosols from Asia and subsequent chemical transformation, *J.*  
10 *Geophys. Res.*, 112, D22S31, doi:10.1029/2006JD008120, 2007.

11 Ueda, S., Osada, K., and Takami, A.: Morphological features of soot-containing particles  
12 internally mixed with water-soluble materials in continental outflow observed at Cape Hedo,  
13 Okinawa, Japan. *J. Geophys. Res.* 116, doi: 10.1029/2010JD015565, 2011.

14 Ueda, S., Hirose, Y., Miura, K., and Okochi, H.: Individual aerosol particles in and below  
15 clouds along a Mt. Fuji slope: Modification of sea-salt-containing particles by in-cloud  
16 processing, *Atmos. Res.*, 137, 216–227, D17207, doi:10.1016/j.atmosres.2010.10.021, 2014.

17 Vester, B. P., Ebert, M., Barnert, E. B., Schneider, J., Kandler, K., Schütz, L., and Weinbruch,  
18 S.: Composition and mixing state of the urban background aerosol in the Rhein-Main area  
19 (Germany), *Atmos. Environ.*, 41, 6102–6115, doi:10.1016/j.atmosenv.2007.04.021, 2007.

20 Weingartner, E., Burtscher, H., and Baltensperger, U.: Hygroscopic properties of carbon and  
21 diesel soot particles, *Atmos. Environ.*, 31, 2311–2327, doi:10.1016/S1352-2310(97)00023-X,  
22 1997.

23 Yang, H. and Yu, Z.: Uncertainties in charring correction in the analysis of elemental and  
24 organic carbon in atmospheric particles by thermal/optical methods, *Environ. Sci. Tech.*, 36,  
25 5199–5204, doi: 10.1021/es025672z, 2002.

26 Yu, J. Z., Xu, J., and Yang, H.: Charring characteristics of atmospheric organic particulate  
27 matter in Thermal Analysis, *Environ. Sci. Tech.*, 36, 754–761, doi:10.1021/es015540q, 2002.

28 Yuba, A., Sadanaga, Y., Takami, A., Hatakeyama, S., Takenaka, N., and Bandow, H.:  
29 Measurement system for particulate nitrate based on the scrubber difference NO-O<sub>3</sub>

1 chemiluminescence method in remote areas, *Anal. Chem.*, 82, 8916–8921, doi:  
2 10.1021/ac101704w, 2010.

3 Yuba, A., Sadanaga, Y., Takami, A., Hatakeyama, S., Takenaka, N., Yoshihiko, M., Ohara, T.,  
4 Yonemura, S., Kato, S., Kajii, Y., and Bandow, H.: Concentration variations of total reactive  
5 nitrogen and total nitrate during transport to Fukue Island and to Cape Hedo, Japan in the  
6 marine boundary layer, *Atmos. Environ.*, 97, 471–478, doi:10.1016/j.atmosenv.2014.04.010,  
7 2014.

8 Zuberi, B., Johnson, K. S., Aleks, G. K., Molina, L. T., and Molina, M. J.: Hydrophilic  
9 properties of aged soot, *Geophys. Res. Lett.*, 32, L01807, doi:10.1029/2004GL021496, 2005.

10

11

1 Table 1. Average values of absorption and scattering coefficients and enhancement of  
 2 absorption during the observation period <sup>a</sup>

$\lambda$	$b_{abs}(\lambda)$	$b_{sca}(\lambda)$	$E_{abs}(\lambda, 300^{\circ}\text{C})^b$	$E_{abs}(\lambda, 400^{\circ}\text{C})^b$
405 nm	3.1 [1.3–4.6]	51.9 [23.5–70.1]	0.98 [0.85–1.09]	0.99 [0.87–1.06]
532 nm	2.7 [1.2–3.8]	---	1.06 [0.90–1.20]	1.06 [0.93–1.20]
781 nm	1.7 [0.8–2.4]	16.1 [7.3–17.4]	1.22 [1.07–1.38]	1.23 [1.10–1.35]

3 <sup>a</sup> Values in square brackets show the 25<sup>th</sup>–75<sup>th</sup> percentile range.

4 <sup>b</sup> Only the data above the detection limit were used in the calculation.

5

1 Table 2. TEM samples used in this study, and rBC, NO<sub>x</sub>, and NO<sub>y</sub> concentrations and optical  
 2 parameters (average values ± standard deviation) during the sampling periods

TEM sample			A	B	C	D
ID						
Date			6-May	10-May	13-May	14-May
Starting local time			9:10	10:09	16:00	8:29
Collection time			7 min	7 min	10 min	6 min
Analyzed particle number			586	296	226	412
SP2						
rBC mass	[ngm <sup>-3</sup> ]		424 ± 11	403 ± 30	520 ± 28	597 ± 21
ACSM						
Org	[μgm <sup>-3</sup> ]		6.20	8.81	-	7.64
NH <sub>4</sub> <sup>+</sup>	[μgm <sup>-3</sup> ]		1.45	1.52	-	5.87
SO <sub>4</sub> <sup>2-</sup>	[μgm <sup>-3</sup> ]		2.02	2.10	-	17.46
NO <sub>3</sub> <sup>-</sup>	[μgm <sup>-3</sup> ]		0.34	1.72	-	1.05
Cl <sup>-</sup>	[μgm <sup>-3</sup> ]		0.03	nd	-	nd
Total mass	[μgm <sup>-3</sup> ]		10.05	14.15	-	32.01
NO <sub>x</sub> , NO <sub>y</sub>						
NO <sub>x</sub>	[ppbv]		1.6 ± 0.9	3.7 ± 1.7	1.3 ± 0.1	1.0 ± 0.1
NO <sub>y</sub>	[ppbv]		3.4 ± 0.9	5.3 ± 1.5	3.5 ± 0.2	4.0 ± 0.2
[NO <sub>x</sub> ]/[NO <sub>y</sub> ]			0.43 ± 0.12	0.67 ± 0.11	0.38 ± 0.03	0.24 ± 0.03
PASS-3						
<i>b</i> <sub>abs</sub>	[Mm <sup>-1</sup> ]	405 nm	6.3 ± 0.6	5.6 ± 1.2	7.9 ± 0.8	9.4 ± 0.2
		532 nm	4.6 ± 2.1	4.4 ± 0.6	6.0 ± 0.6	8.2 ± 0.4
		781 nm	2.8 ± 0.3	1.9 ± 0.6	3.5 ± 0.6	4.7 ± 0.2
<i>b</i> <sub>sca</sub>	[Mm <sup>-1</sup> ]	405 nm	99.8 ± 7.4	79.0 ± 4.1	155.8 ± 5.0	215.1 ± 1.9
		781 nm	27.3 ± 4.7	35.6 ± 17.3	69.2 ± 2.9	120.7 ± 2.5
<i>E</i> <sub>abs</sub> (300°C)		405 nm	0.88 ± 0.12	0.97 ± 0.26	1.33 ± 0.21	1.35 ± 0.06
		532 nm	1.31 ± 0.60	1.09 ± 0.40	1.42 ± 0.24	1.18 ± 0.20
		781 nm	1.25 ± 0.37	1.13 ± 0.49	1.44 ± 0.23	1.42 ± 0.18
<i>E</i> <sub>abs</sub> (400°C)		405 nm	0.88 ± 0.12	1.03 ± 0.25	1.22 ± 0.13	1.31 ± 0.06
		532 nm	1.05 ± 0.15	1.13 ± 0.36	1.10 ± 0.12	1.43 ± 0.38
		781 nm	1.26 ± 0.29	1.24 ± 0.60	1.58 ± 0.20	1.52 ± 0.19

4  
5

1 Table 3. Parameters of the soot-containing particles of TEM samples <sup>a</sup>

ID		Number of soot particles	Particle diameter $d_p$ [ $\mu\text{m}$ ]	Soot diameter $d_s$ [ $\mu\text{m}$ ]	Volume fraction of soot $VF_s$ [%]	Relative position of soot $RP$	Circularity factor $CF$	Aspect ratio $AR$
A	<0.6 $\mu\text{m}$	99	0.36 [0.26-0.45]	0.22 [0.16-0.25]	33 [10-50]	0.55 [0.30-0.74]	0.73 [0.59-0.93]	1.4 [1.1-1.6]
	>0.6 $\mu\text{m}$	10	0.83 [0.67-0.83]	0.36 [0.28-0.42]	11 [6-14]	0.89 [0.75-1.02]	0.34 [0.26-0.40]	2.1 [1.8-2.4]
B	<0.6 $\mu\text{m}$	33	0.36 [0.26-0.47]	0.20 [0.15-0.24]	50 [7-55]	0.48 [0.29-0.68]	0.60 [0.52-0.73]	1.4 [1.2-1.5]
	>0.6 $\mu\text{m}$	18	0.89 [0.73-1.07]	0.37 [0.21-0.55]	13 [2-16]	0.61 [0.42-0.79]	0.39 [0.21-0.56]	1.4 [1.2-1.5]
C	<0.6 $\mu\text{m}$	6	0.58 [0.57-0.59]	0.32 [0.22-0.40]	21 [5-31]	0.42 [0.28-0.58]	0.86 [0.84-0.88]	1.2 [1.1-1.2]
	>0.6 $\mu\text{m}$	75	0.92 [0.73-1.04]	0.33 [0.22-0.37]	9 [2-10]	0.44 [0.24-0.64]	0.81 [0.75-0.92]	1.2 [1.1-1.4]
D	<0.6 $\mu\text{m}$	86	0.47 [0.42-0.51]	0.23 [0.17-0.30]	22 [5-27]	0.55 [0.25-0.66]	0.89 [0.87-0.94]	1.1 [1.0-1.2]
	>0.6 $\mu\text{m}$	80	0.87 [0.71-1.02]	0.28 [0.14-0.35]	10 [1-12]	0.63 [0.38-0.87]	0.80 [0.70-0.92]	1.3 [1.1-1.5]

2 <sup>a</sup> Values in square brackets are show the 25<sup>th</sup>–75<sup>th</sup> percentile values

3

1 Table 4. Number fraction of mixing type of soot for soot-containing particles [%]

ID	Type a	Type c	
		Attached/partl y-embedded	coated
A	<0.6 $\mu$ m	9	62
	>0.6 $\mu$ m	0	30
B	<0.6 $\mu$ m	12	55
	>0.6 $\mu$ m	0	39
C	<0.6 $\mu$ m	0	100
	>0.6 $\mu$ m	0	83
D	<0.6 $\mu$ m	0	95
	>0.6 $\mu$ m	0	90

2

## 1 **Figure Captions**

2 Figure 1. Flow diagram of a measurement system for dried particles that did and did not pass  
3 through the **thermodenuders** (TDs) maintained at 300 and 400 °C using the PASS-3, SMPS,  
4 and SP2. Black arrow lines indicate the flow lines of sample air.

5 Figure 2. Temporal variations in (a) absorption coefficients at 405 nm and start times of TEM  
6 sampling (A–D with arrows), (b) scattering coefficients at 405 nm, (c) absorption  
7 coefficients at 781 nm, (d) scattering coefficients at 781 nm, and (e, f and g) enhancement of  
8 light absorption ( $E_{\text{abs}}$ ) at 405, 532 and 781 nm, respectively. Red, blue, and green symbols in  
9 (a–d) represent conditions of 25, 300 and 400 °C, respectively. Blue and green symbols in  
10 (e–g) represent  $E_{\text{abs}} [= b_{\text{abs}}(\lambda, 25^{\circ}\text{C})/b_{\text{abs}}(\lambda, T)]$  with  $T = 300$  and  $400$  °C, respectively. **The**  
11 **values are 3-h averaged data.**

12 Figure 3. (a) Location of NOTOGRO in Ishikawa, Japan and (b–e) 72-hour backward air  
13 trajectories for air masses reaching the observation site at 500 m above sea level. These are  
14 colored with (b)  $b_{\text{abs}}(405 \text{ nm})$ , (c)  $b_{\text{abs}}(781 \text{ nm})$ , (d)  $E_{\text{abs}}(405 \text{ nm})$  and (e)  $E_{\text{abs}}(781 \text{ nm})$ . The  
15 trajectories for  $E_{\text{abs}}$  calculated from  $b_{\text{abs}}$  data below the detection limit are represented as thin  
16 lines in (d) and (e).

17 Figure 4. The 72-hour horizontal backward trajectories for air masses reaching the  
18 observation site at 500 m above sea level during sampling periods A–D. Open dots along the  
19 trajectory represent the position of the air mass every 24 hour backward from the arrival  
20 point.

21 Figure 5. Number- (upper panels), cross-section area- and volume-based (lower panels) size  
22 distributions of aerosol particles during the sampling of samples A–D, as measured by SMPS.  
23 Red lines in the upper panels represent the number-based size distributions for particles  
24 measured without passage through the **TD**, while blue and green lines represent those for  
25 particles measured after passage through the **TD** maintained at 300 and 400 °C, respectively.

26 Figure 6. (a) Mass-based size distributions of rBC with log-normal best-fitting curves and (b)  
27 normalized-count distribution of lag time of the incandescent-light signal from the scattering  
28 signal for rBC with a mass equivalent diameter of 200 nm, obtained using the SP2 for  
29 samples A–D with best fit curves assuming the combination of two Gaussian functions. LT  
30 represents averaged lag-time.

1 Figure 7. Electron microphotographs before and after EDS analysis of samples (a, a') A and  
2 (b, b') D. Soot is shown by black triangles in (a') and (b'). Non-soot residues are shown by  
3 white triangles.

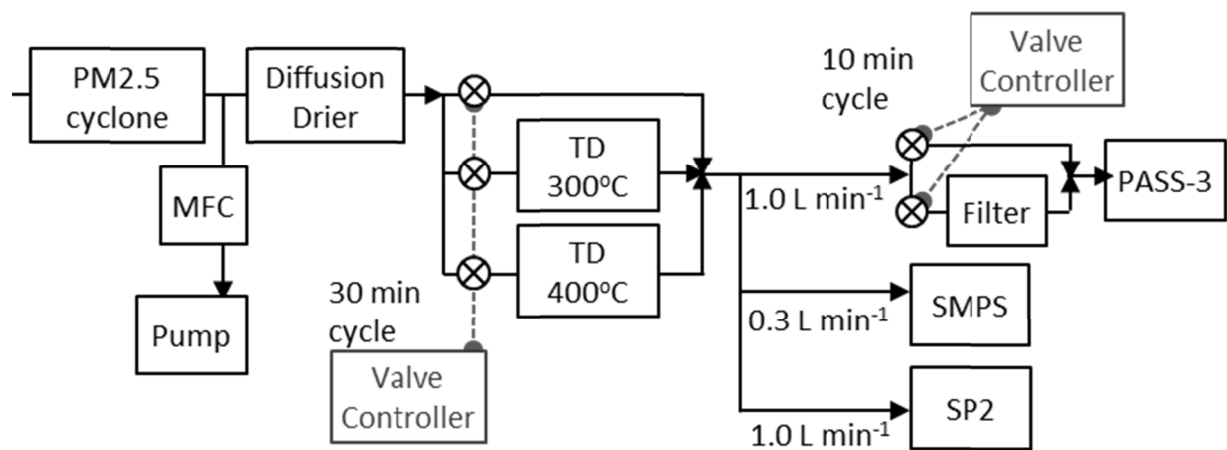
4 Figure 8. Morphological classification of particle types 1–7. Horizontal bars in the  
5 photographs represent a length of 0.5  $\mu\text{m}$ . The pie chart in each morphological type  
6 represents the number fraction of compositional types classified based on the EDS analysis.  
7 The number below the pie chart represents the number of analyzed particles.

8 Figure 9. Classification of mixing states based on the comparison of electron micrographs for  
9 individual particles before (left) and after (right) irradiation by a high, densely electron  
10 beam: type *a*, non-volatile soot particles; type *b*, non-volatile particles except soot; type *c*,  
11 mixed particles of volatile material and non-volatile soot aggregate; type *d*, mixed particles  
12 of volatile material and non-volatile core without a soot-like shape; type *e*, semi-volatile  
13 particles; and type *f*, volatile particles. The pie chart in each mixing state type *a–f* represents  
14 the number fraction of compositional types determined by EDS analysis.

15 Figure 10. Size-segregated number proportions of (a) mixing state particle types on the basis  
16 of the classification in Figure 9, (b) morphological particle types on the basis of the  
17 classification in Figure 8 and (c) morphological particle types of soot-containing particles for  
18 samples A–D. The numbers above the columns show the number of particles observed.

19 Figure 11. Photographs of an aerosol sample after passage through the TD at 400°C sampled  
20 for 10 min from 09:38 May 6 (LT).

21



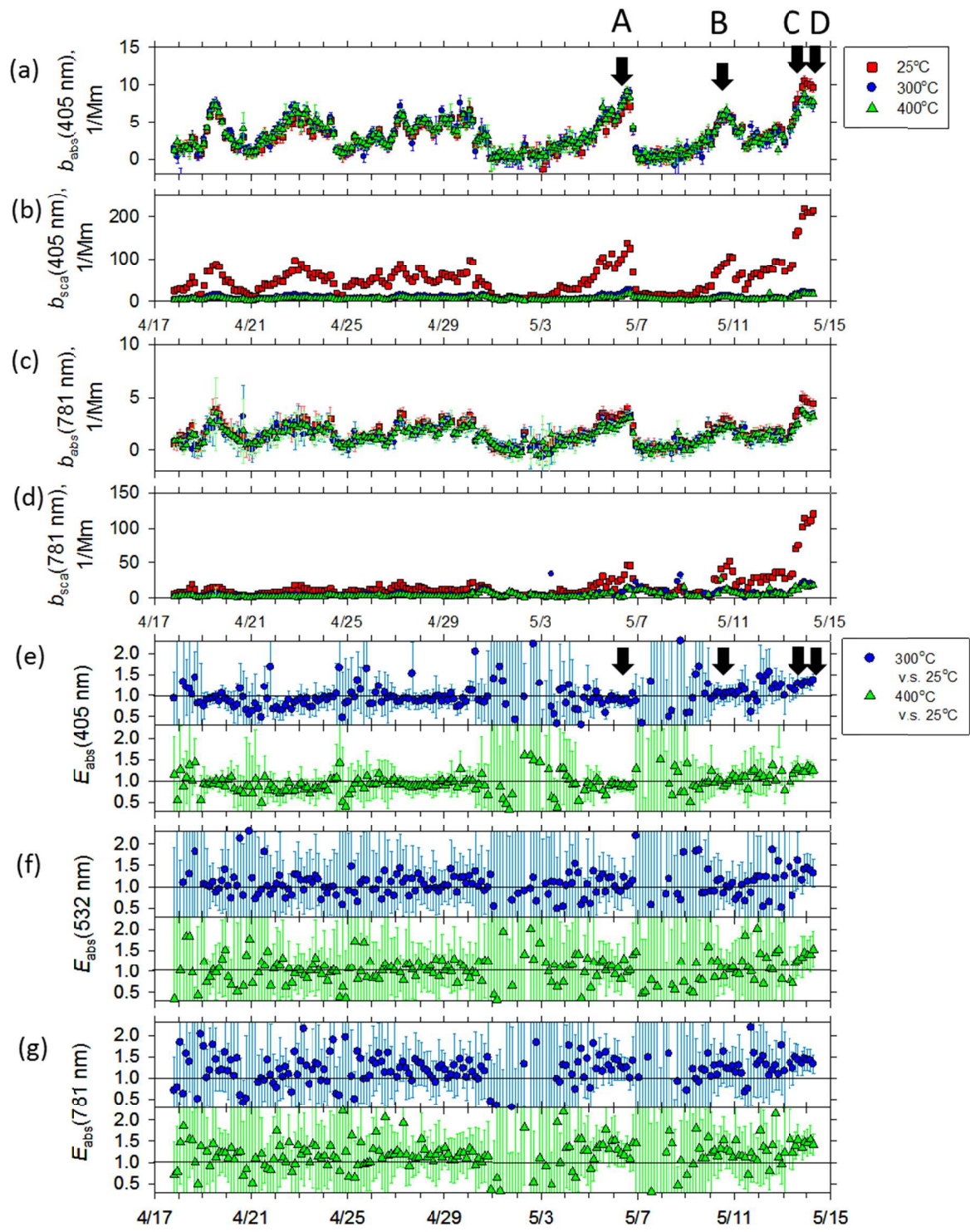
1

2

3 **Figure 1.**

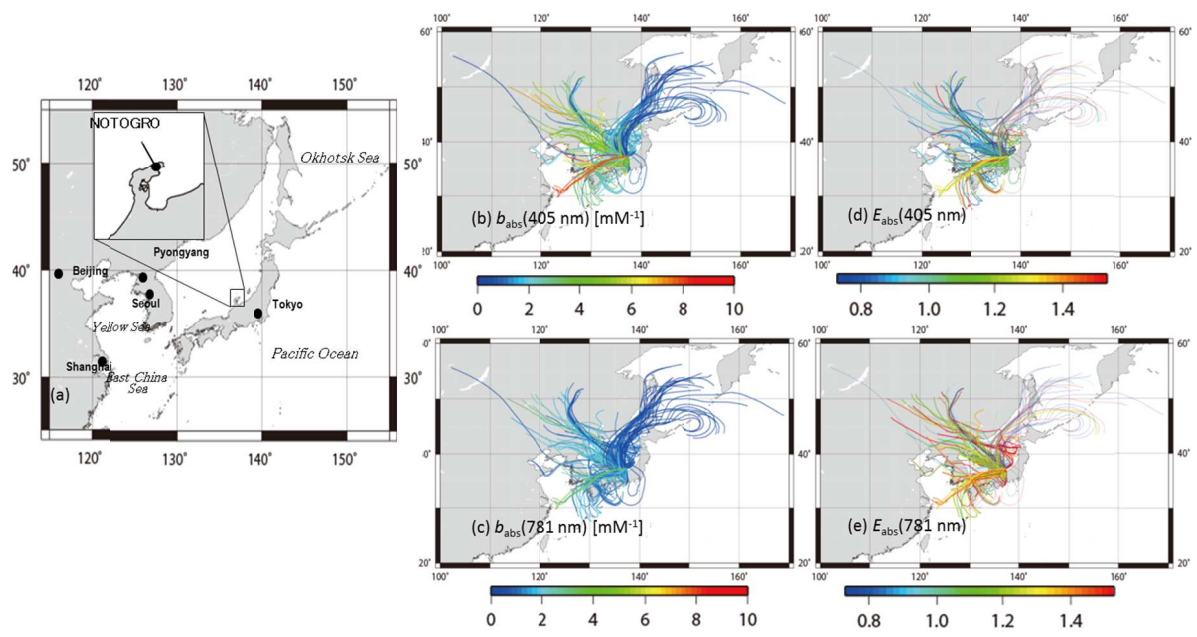
4

5



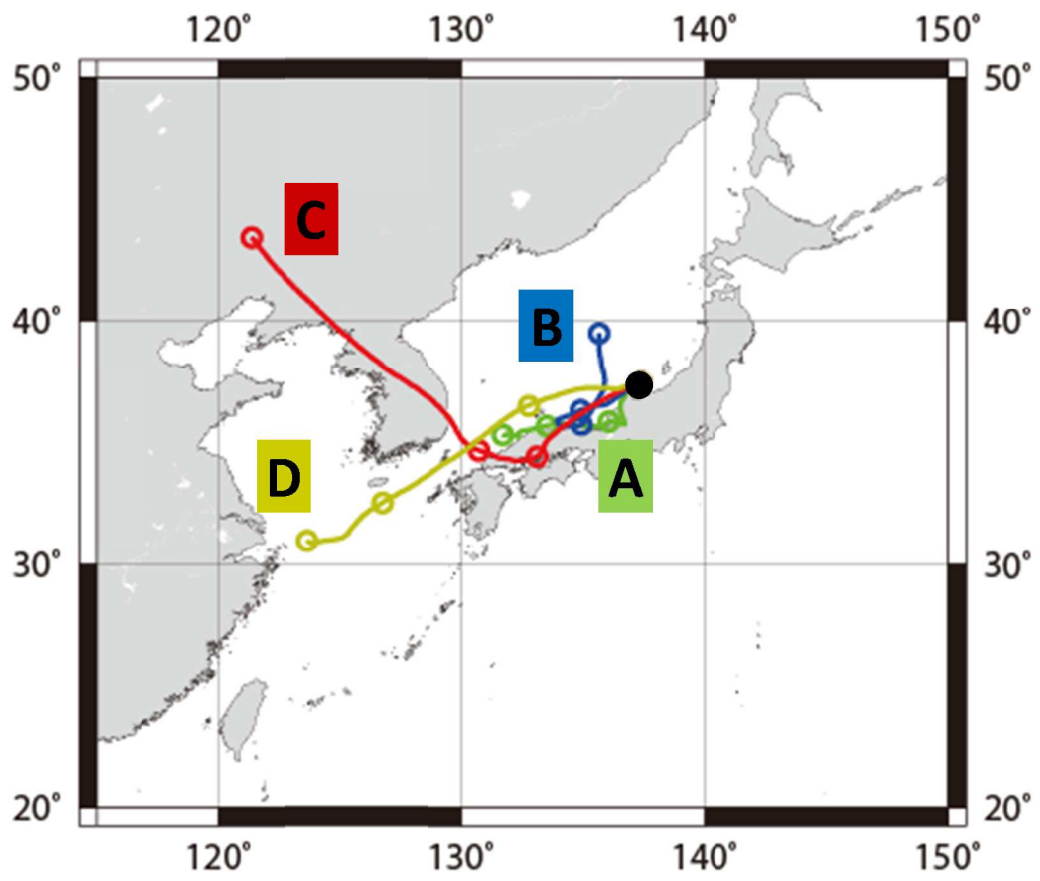
1  
2  
3  
4  
5

Figure 2.



- 1
- 2
- 3
- 4
- 5

Figure 3.

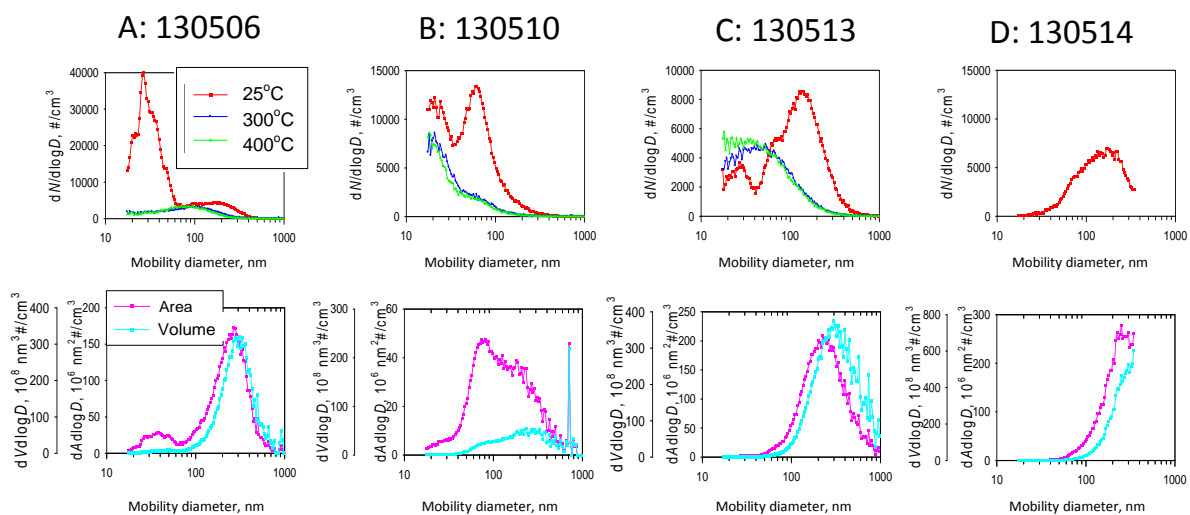


1

2 Figure 4.

3

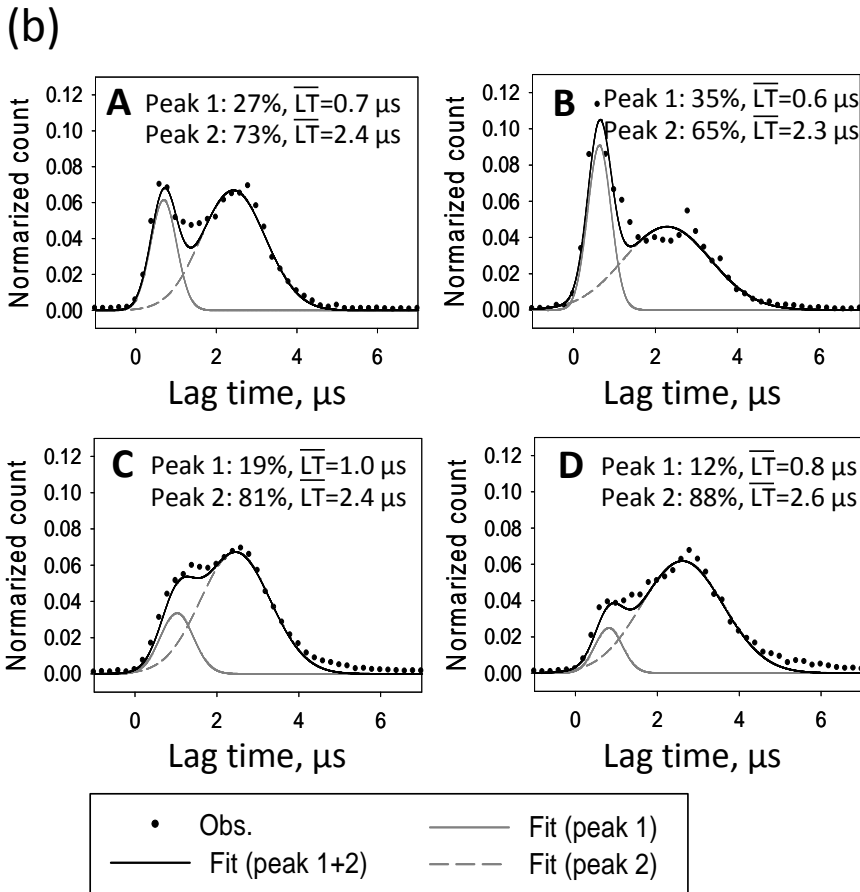
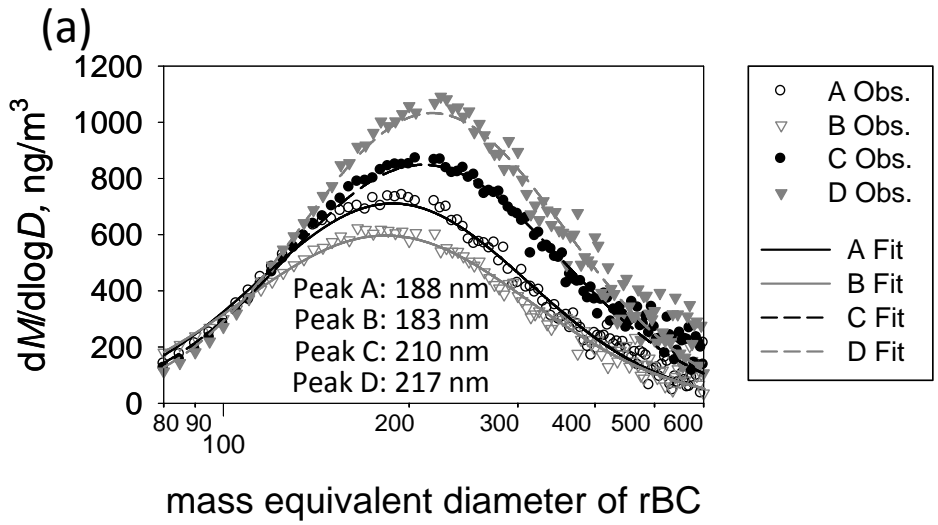
1



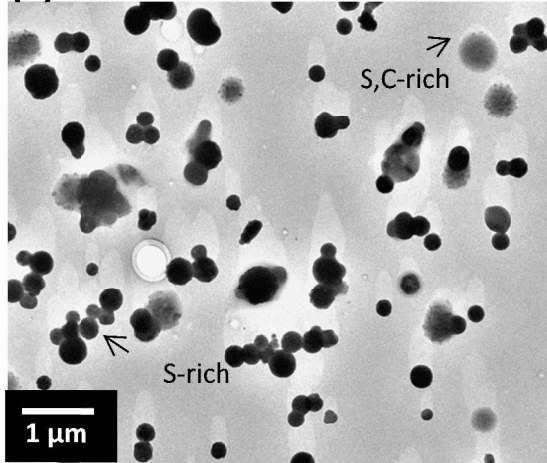
2

3 Figure 5.

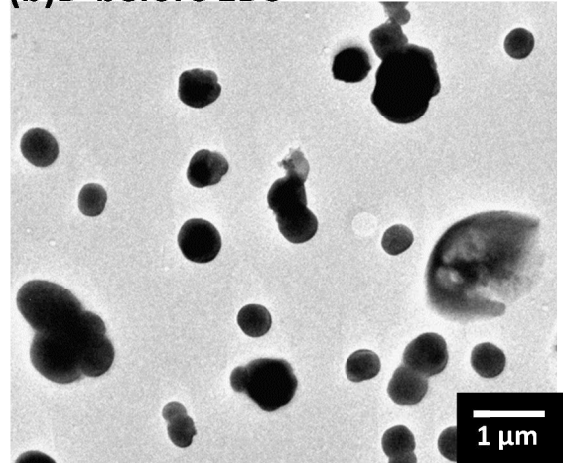
4



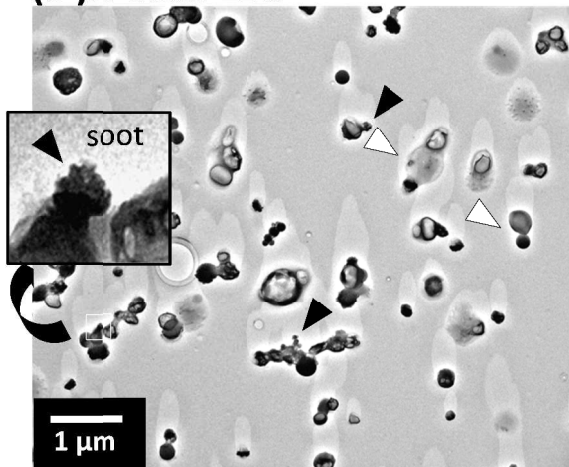
(a)A-before EDS



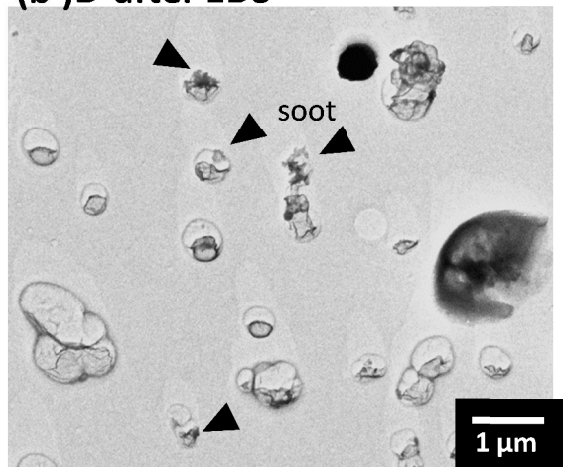
(b)D-before EDS



(a')A-after EDS



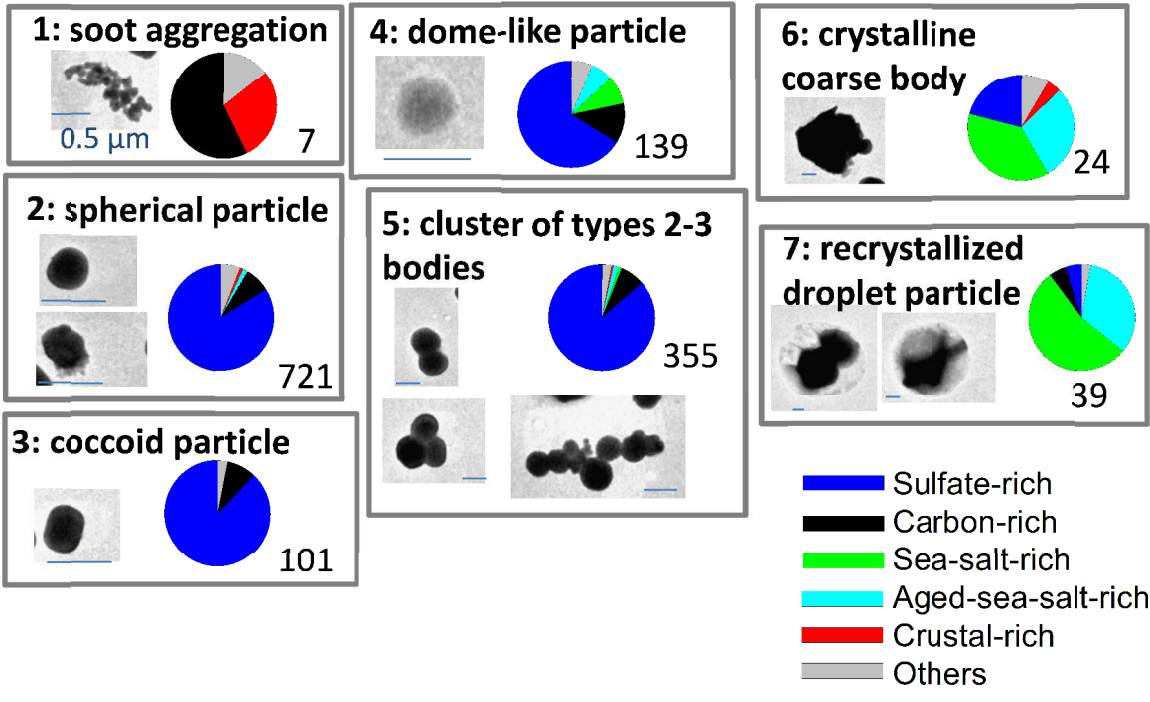
(b')D-after EDS



1  
2  
3  
4

Figure 7.

# Morphological Types



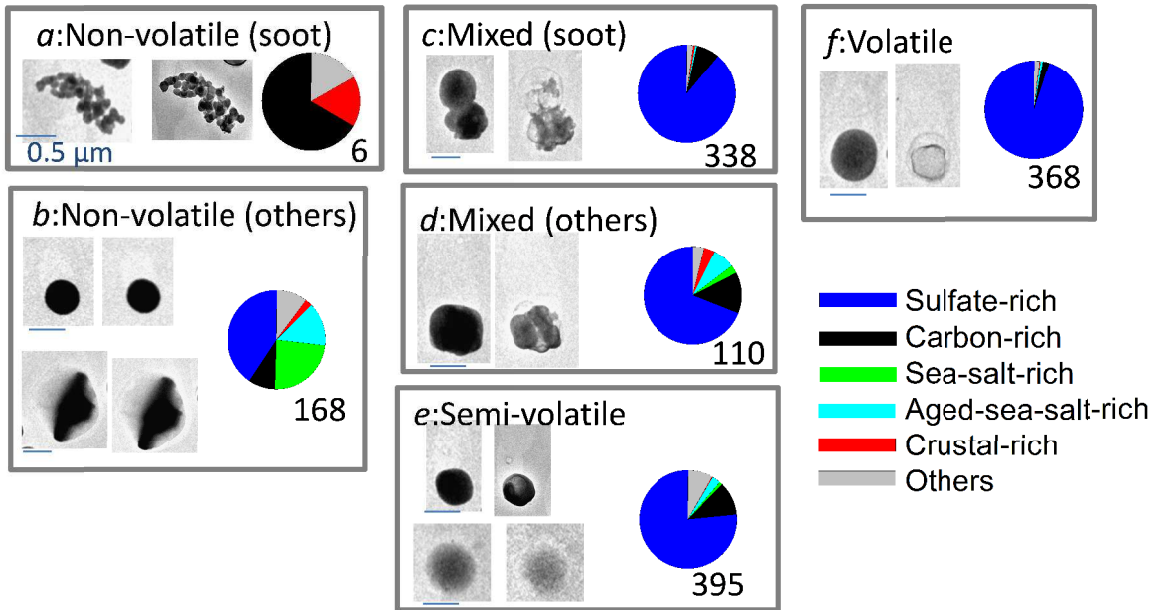
1

2 Figure 8.

3

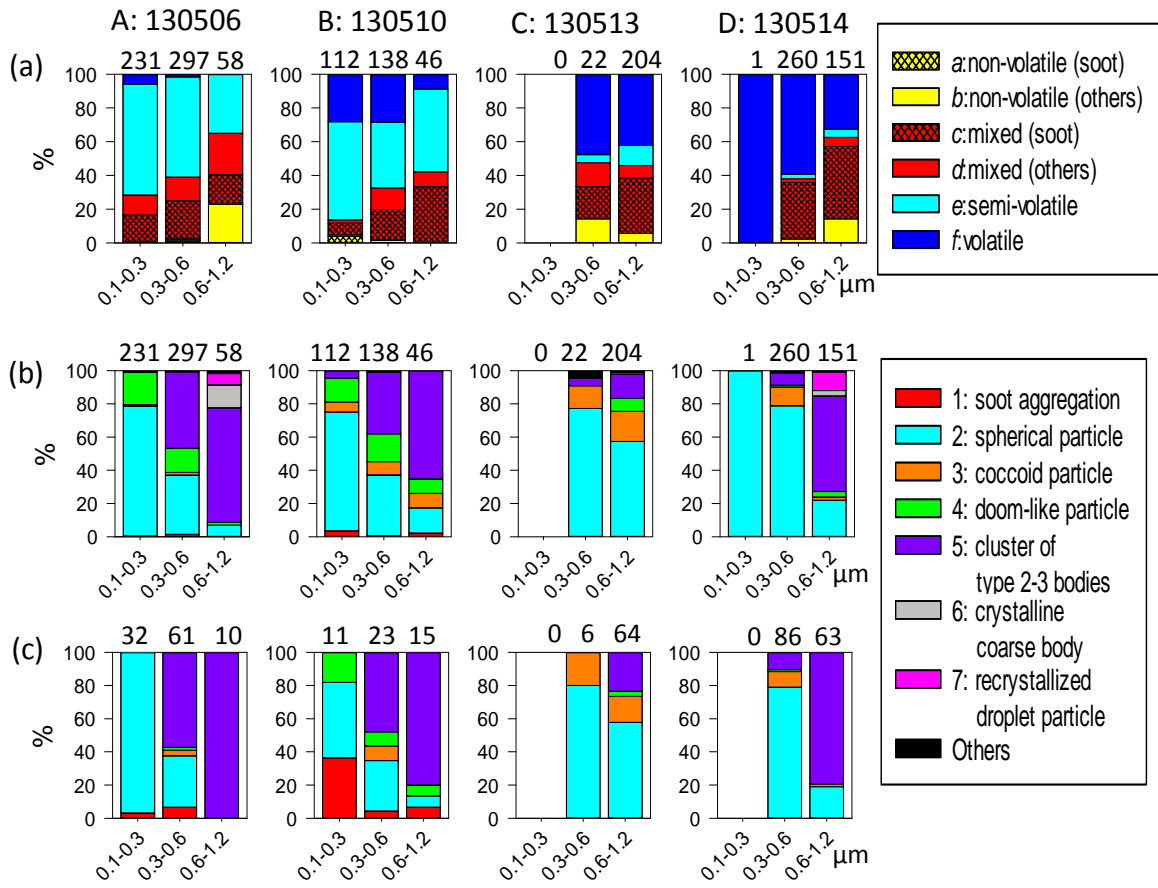
# Mixing state type

Before (left) & After (right) EDX



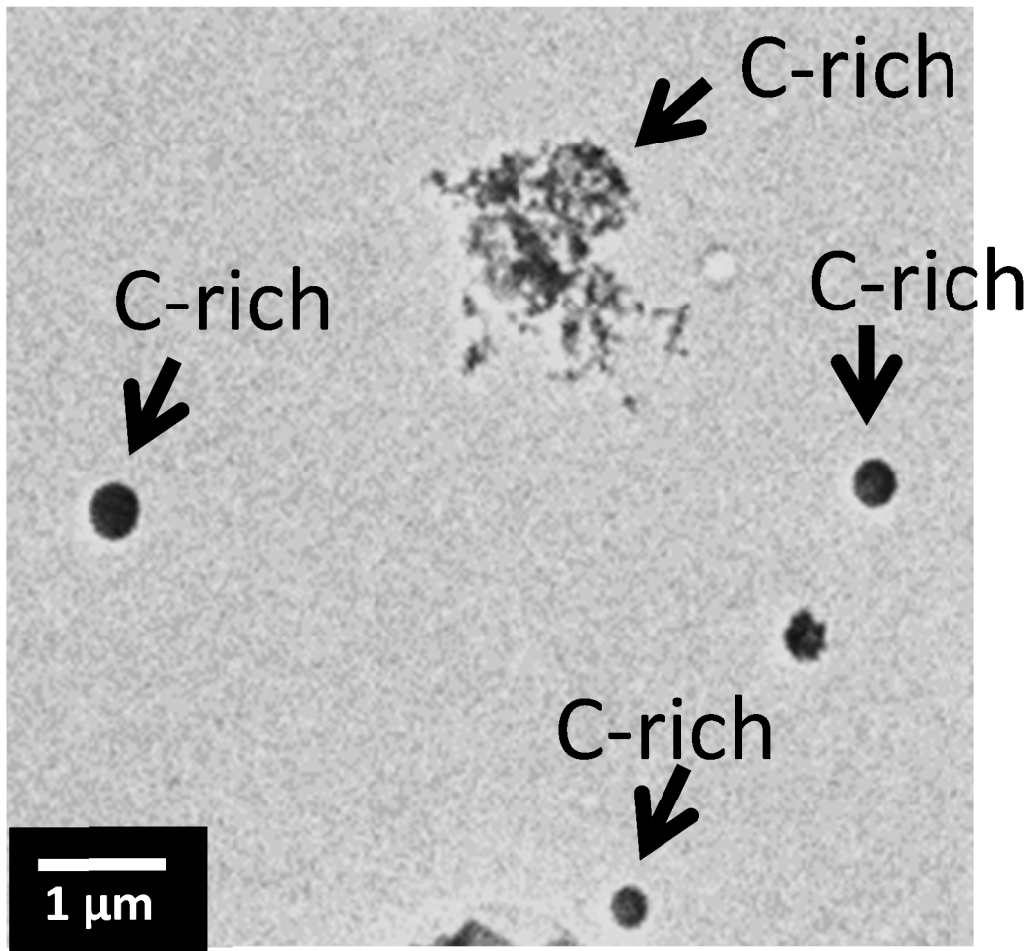
1  
2  
3  
4

Figure 9.



1  
2  
3  
4

Figure 10.



1

2

3 Figure 11.

1 *Supplement for*

2 **Light absorption and morphological properties of soot-**  
3 **containing aerosols observed at an East Asian outflow site,**  
4 **Noto Peninsula, Japan**

5 **S. Ueda<sup>1,2</sup>, T. Nakayama<sup>1,3</sup>, F. Taketani<sup>4</sup>, K. Adachi<sup>5</sup>, A. Matsuki<sup>6</sup>, Y. Iwamoto<sup>6,7</sup>, Y.**  
6 **Sadanaga<sup>8</sup> and Y. Matsumi<sup>1,3</sup>**

7 [1]{Solar-Terrestrial Environment Laboratory, Nagoya University, Nagoya, Japan}

8 [2] {Now at Graduate School of Environmental Studies, Nagoya University, Nagoya, Japan}

9 [3] {Now at Institute for Space-Earth Environmental Research, Nagoya University, Nagoya,  
10 Japan}

11 [4]{Japan Agency for Marine-Earth Science and Technology, Yokohama, Japan}

12 [5]{Atmospheric Environment and Applied Meteorology Research Department,  
13 Meteorological Research Institute, Tsukuba, Japan}

14 [6]{Institute of Nature and Environmental Technology, Kanazawa University, Kanazawa,  
15 Japan}

16 [7]{Now at Faculty of Science Division I, Tokyo University of Science, Tokyo, Japan}

17 [8]{Graduate School of Engineering, Osaka Prefecture University, Osaka, Japan}

18

19 Correspondence to: S. Ueda ([ueda-s@stelab.nagoya-u.ac.jp](mailto:ueda-s@stelab.nagoya-u.ac.jp)) and T. Nakayama  
20 ([nakayama@stelab.nagoya-u.ac.jp](mailto:nakayama@stelab.nagoya-u.ac.jp))

21

22 **S1 Collection efficiency of the ACSM**

23 A collection efficiency (CE) of the ACSM was determined by comparing the mass  
24 concentrations of ammonium and sulfate derived by the ACSM to those measured by a  
25 conventional filter based off-line chemical analysis. The filter samples were collected using a  
26 9-stage Andersen sampler (model AN-200, Tokyo Dylec corp.) with a flow rate of 28.3 L/min.  
27 Sampling duration was 1 week per sample. The filters were extracted and water soluble  
28 inorganic components were analyzed by ion chromatography. Ammonium and sulfate

1 concentrations were integrated for the smallest 3 stages (including backup filter) to get the  
2 PM1.1 fraction. The CE was tuned so that the ACSM derived ammonium and sulfate match  
3 the filter based analysis.

4 In addition, volume concentrations of NR components were calculated using the ACSM data  
5 using the same procedure with our previous study (Nakayama et al. 2014), and were  
6 compared to volume concentrations estimated using the SMPS data (TSI, model 3936L72).  
7 As a result, the volume concentrations estimated from SMPS data were found to be about 1.7  
8 times larger than those calculated from ACSM data. While different size-cut profiles of the  
9 ACSM, Andersen sampler, and SMPS may have affected the result, measurement uncertainty  
10 of SMPS may also contribute to the difference.

## 12 **S2 Morphological types of individual particles**

13 Based on TEM image analysis, the particles were classified into seven types based on their  
14 morphological features, as presented in Figure 8.

15 Particles classified as type 1 are aggregations of globules with a diameter less than 50 nm,  
16 which is characteristic of soot particles (Janzen, 1980; Pósfai et al., 2004; Murr and Soto,  
17 2005). The results of the EDS analysis suggested that particles in this type were composed  
18 mainly of carbon.

19 Particles of types 2 and 3 are, respectively, single spherical and single coccoid (having  
20 parallel straight lines for the particle perimeter). These particles showed strong contrast with  
21 the film, suggesting that they are thick or highly crystalline. Because the length of the Pt/Pd  
22 shadow of these particles is long (i.e., comparable to the particle diameter), it can be inferred  
23 that these were collected on the film as solid particles. According to results of the EDS  
24 analysis, type 2 and 3 particles were mostly sulfate-rich. Similar coccoid shaped sulfate  
25 particles have been reported by several studies on aerosols in urban regions and an Asian  
26 outflow (Li and Shao, 2010; Ueda et al., 2011), as well as aerosols emitted from biomass  
27 burning (Li et al., 2003). These workers identified such particles as ammonium sulfate  
28 particles based on selected-area electron diffraction analysis.

29 Type 4 particles have a spherical cap and show weak contrast to the collection film and a  
30 short Pt/Pd shadow. The short shadow length suggests a dome shape, implying that the

1 particles were not solid when sampled. Most type 4 particles are rich in sulfur, and several of  
2 them were rich in carbon or sea-salt.

3 Type 5 particles are clustered, connected to form numerous spherical or coccoid units  
4 resembling type 2 or 3 particles in shape and size (0.2–0.5  $\mu\text{m}$  diameter). Most type 5  
5 particles in this study were also sulfate-rich.

6 Type 6 particles are crystalline coarse particles having some straight lines for the particle  
7 perimeter, but an otherwise coccoid shape. These particles have larger diameters (around 1  
8  $\mu\text{m}$ ) than type 3. Most of the type 6 particles were sea salt-rich or aged sea salt-rich particles.

9 Type 7 particles are recrystallized droplet particles. They show a short Pt/Pd shadow, similar  
10 to type 4 particles, but partially show a strong contrast with the collection film. These results  
11 imply that they dried on the film after their collection as liquid particles. Most type 7 particles  
12 were also sea salt-rich or aged sea salt-rich.

13 The volume-equivalent diameters of each particle were calculated from measurements of the  
14 projected particle area  $S$ . For type 1, 2, 3, 5 and 6 particles, which were considered to be solid  
15 at the time of their collection, the particle diameter  $d$  was defined as  $2(S/\pi)^{1/2}$ . For types 4 and  
16 7, which were considered as liquid droplets at the time of their collection,  $d$  was defined as  
17  $2^{2/3}(S/\pi)^{1/2}$  by assuming half-sphere.

18

### 19 **S3 Mixing states of individual particles**

20 The mixing states of particles were classified by comparing particle morphology before and  
21 after irradiation by the intense electron beam of the EDS analysis. The types of mixing states  
22 are shown in Figure 9. Type *a* is non-volatile soot particles, which have the characteristic  
23 shape of soot (i.e., morphological type 1) and show no change in morphological appearance  
24 after irradiation by electron beam. Type *b* is non-volatile particles without the characteristic  
25 shape of soot. Type *c* is mixed particles of beam-sensitive material and non-volatile soot  
26 aggregate. Type *d* is mixed particles of beam-sensitive material and a non-volatile core,  
27 without the characteristic shape of soot. Type *e* is semi-volatile particles. Although contrasts  
28 of the type *e* particles decrease overall after irradiation by a high electron beam, the area does  
29 not change. In contrast to types *b* and *c*, type *e* particles do not have a non-volatile core. Type  
30 *f* is volatile particles.

1

## 2 **S4 Internal mixing states and shape factors for soot-containing particles**

3 The shape factors for soot-containing particles were estimated by electron micrographs before  
4 and after irradiation with an intense electron beam. Figure S1 shows examples of electron  
5 microphotographs of a soot-containing particle before and such irradiation together with their  
6 shape factors determined in this study. The projected area ( $A_p$ ), perimeter ( $L_p$ ), length of  
7 longest axis ( $a$ ), right-angled length to longest axis ( $b$ ), and coordinates of folding center ( $x_p$ ,  
8  $y_p$ ) of soot-containing particles before EDS analysis, and the projected area ( $A_s$ ) and  
9 coordinates of folding center ( $x_s$ ,  $y_s$ ) of soot in the particle after EDS analysis were measured  
10 using image analysis software. Using these, six parameters for soot-containing particles  
11 (particle and soot diameters ( $d_p$  and  $d_s$ ), volume fraction and relative position of soot ( $VF_s$  and  
12  $RP$ ), circularity factor ( $CF$ ), and aspect ratio ( $AR$ )) were estimated based on the equation  
13 shown in Table S1. The  $CF$  and  $AR$  represent shape factors; their values for a circle are 1,  
14 while for irregular shapes are less than 1 and higher than 1, respectively. The  $RP$  is an  
15 indicator of soot position in the particle. Values of 0, 1, and  $> 1$  mean that the soot is in the  
16 center of the soot-containing particle, in a position equal to the sphere-equivalent diameter  
17 from the particle center, or outside of the sphere-equivalent diameter from the particle center,  
18 respectively.

19

## 20 **References**

- 21 Janzen, J.: Extinction of light by highly nonspherical strongly absorbing colloidal particles:  
22 spectrophotometric determination of volume distributions for carbon blacks, *Appl. Opt.*, 19,  
23 2977–2985, doi: 10.1364/AO.19.002977, 1980.
- 24 Li, J., Pósfai, M., Hobbs, P. V., and Buseck, P. R.: Individual aerosol particles from biomass  
25 burning in southern Africa: 2, Compositions and aging of inorganic particles, *J. Geophys.*  
26 *Res.*, 108, D13, 8484, doi:10.1029/2002JD002310, 2003.
- 27 Li, W. and Shao, L.: Mixing and water-soluble characteristics of particulate organic  
28 compounds in individual urban aerosol particles, *J. Geophys. Res.*, 115, D02301,  
29 doi:10.1029/2009JD012575, 2010.

1 Murr, L. E. and Soto, K. F.: A TEM study of soot, carbon nanotubes, and related fullerene  
2 nanopholyhedra in common fuel-gas combustion sources, *Mater. Charact.*, 55, 50–65. 2005.

3 Nakayama, T., Ikeda, Y., Sawada, Y., Setoguchi, Y., Ogawa, S., Kawana, K., Mochida, M.,  
4 Ikemori, F., Matsumoto, K., and Matsumi, Y.: Properties of light-absorbing aerosols in the  
5 Nagoya urban area, Japan, in August 2011 and January 2012: Contributions of brown carbon  
6 and lensing effect, *J. Geophys. Res. Atmos.*, 119, 12721–12739, doi:10.1002/2014JD021744,  
7 2014.

8 Pósfai, M., Gelencser, A., Simonics, R., Arato, K., Li, J., Hobbs, P. V., and Buseck, P. R.:  
9 Atmospheric tar balls: Particles from biomass and biofuel burning, *J. Geophys. Res.*, 109,  
10 D06213, doi: 10.1029/2003JD004169, 2004.

11 Ueda, S., Osada, K., and Takami, A.: Morphological features of soot-containing particles  
12 internally mixed with water-soluble materials in continental outflow observed at Cape Hedo,  
13 Okinawa, Japan. *J. Geophys. Res.* 116, doi: 10.1029/2010JD015565, 2011.

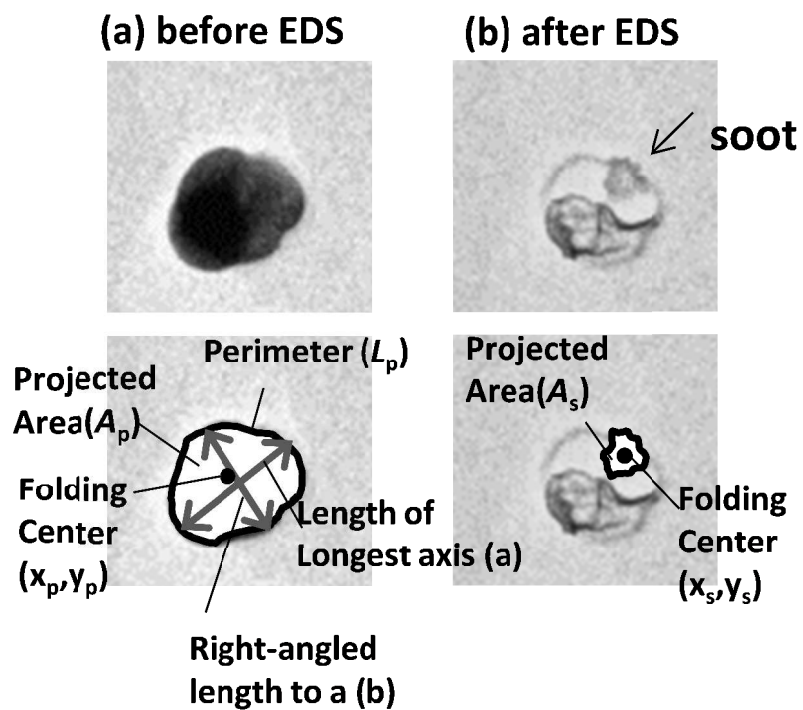
14  
15

1 Table S1. Parameter descriptions of soot-containing particles by image analysis.

Parameter	Symbol	Equation
Particle diameter	$d_p$	$d_p = 2(A_p/\pi)^{1/2}$ for type 1, 2, 3, 5 and 6 particles $d_p = 2^{2/3}(A_p/\pi)^{1/2}$ for type 4 and 7 particles
Soot diameter	$d_s$	$d_s = 2(A_s/\pi)^{1/2}$
Volume fraction of soot	$VF_s$	$VF_s = (d_s/d_p)^3$
Relative position of soot	$RP$	$RP = 2[(x_p - x_s)^2 + (y_p - y_s)^2]^{1/2} / d_p$
Circularity factor	$CF$	$CF = 4\pi A_p / L_p^2$
Aspect ratio	$AR$	$AR = a/b$

2

3



- 1
- 2 Figure S1 Photographs and shape parameters of projection area of soot-containing particles
- 3 before (a) and after (b) irradiation by high density electron beam.